Constraining double neutron star binary evolution from the spatial distribution of short gamma-ray bursts

Oscar Andersson

Lund Observatory
Lund University

2019-EXA154

Degree project of 15 higher education credits
June 2019

Supervisor: Ross Church

Lund Observatory
Box 43
SE-221 00 Lund
Sweden

Abstract

Short gamma-ray bursts are often observed at large spatial offsets from their host galaxies. Neutron star mergers in double neutron star binaries have also recently been confirmed as a progenitors of short gamma-ray bursts (Abbott et al. 2017). We attempt to constrain uncertainties in the evolution of burst-producing neutron star binaries by generating a distribution of burst offsets from the neutron star natal kick, and then compare to a population of observed offsets in spiral galaxies. In order to do so, we model the dynamical effects of the formation of the second neutron star in a double neutron star binary. We find the resulting binary velocity and the time it takes for the binary to merge. Using the velocity and lifetime, we then integrate the trajectories of the binaries within the environment of a spiral galaxy until they merge. It is found that binaries need to be separated by $\lesssim 20$ $R_\odot$ before the supernova to produce a burst within Hubble time. No constraints were found on exploding star mass or kick strength. We also find that kick strengths much weaker (rms ≈ 50 km/s) than kicks derived from isolated pulsars (rms ≈ 500 km/s) could potentially produce all offsets in the probed population of observed binaries.

Populärvetenskaplig beskrivning

Bland de mest kraftfulla händelser som människor har observerat är gammablixtar. Blixtarna är korta utbrott av gammastrålning som ibland dyker upp i rymden. Forskare har länge misstänkt att kollisioner mellan neutronstjärnor ligger bakom en kategori av blixtar, de korta gammablixtarna. För några år sedan bekräftades forskarnas misstankar. De kunde då, med det nya LIGO-observatoriet, observera gravitationsvågor från en kollision mellan neutronstjärnor samtidigt som de också såg en gammablixt från samma del av himlen.

Neutronstjärnor är en exotisk typ av stjärnor som föds i explosiva supernovor när massiva stjärnor dör. De är också de mest kompakta föremålen i universum. Medan de har en diameter på endast några enstaka mil, är de mer massiva än solen – en matsked av en neutronstjärna väger mer än 1000 ton.

Att två neutronstjärnor skulle slumpmässigt kollidera händer inte – det är inte ens astronomiskt osannolikt. Rymden är helt enkelt för stor: forskare förväntar inte att det kommer ske någon kollision mellan stjärnor när vår Vintergata kolliderar med Andromedagalaxen om några miljarder år. För att en kollision mellan neutronstjärnor ska ske, måste de vara bundna till varandra i ett binärsystem, precis som jorden är bunden till solen.

Det är inte enkelt för två stycken neutronstjärnor att hamna i en binär. De genomgår flera komplicerade stadier, samtidigt som de måste överleva båda de två supernovor som de föds i. Från dessa explosioner får binären en spark, vilket gör att de färdas upp till flera tiotusentals ljusår från platsen de föds – vilket stämmer överens med de gammablixtar vi har observerat.

Vi kan göra modeller av hur binären påverkas av supernova-explosioner, och hur den sen färdas genom rymden. Vi kan då förutsäga var neutronstärnorna kommer kollidera och jämföra med var vi ser korta gammablixtar. Genom att göra detta kan vi bättre förstå de komplicerade stadierna som pågår i binären, och även supernovorna som neutronstjärnor föds i.

Contents

List of Figures

List of Tables

Chapter 1

Introduction

Gamma ray bursts (GRB) are short, highly energetic, non-repeating flashes of gamma rays followed by an afterglow. GRBs have a bimodal distribution in their durations, separating them into two distinct populations: the short gamma-ray bursts (SGRB) and the long gamma-ray bursts (LGRB) with a separation at ~ 2 seconds (Kouveliotou et al. 1993). This distinction of two different populations point to SGRBs and LGRBs being different phenomena, with different progenitors.

SGRBs and LGRBs are not just different in their durations, but also where they are found. LGRBs are exclusively found in star-forming galaxies, while SGRBs have been observed in all types of galaxies as well as at large spatial offsets from their host galaxies (Fong et al. 2010). This points to the progenitors of SGRBs being older than the progenitors of LGRBs, and that the SGRB progenitors can travel far from their place of birth.

Neutron star mergers have long been seen as a candidate progenitor of SGRBs (Ruderman 1975). The timescale, down to 10^{-4} s, as well as predictions of the energetics of the merger event, both fit. Furthermore, the natal kicks of neutron stars would also explain the large offsets that have been observed. The coincident observation of a SGRB with the Laser Interferometer Gravitational-Wave Observatory (LIGO) detection of the gravitational wave emission from the merger of two neutron stars (Abbott et al. 2017) finally confirmed neutron star mergers as a progenitor to SGRBs.

Neutron stars are the stellar remnants of massive stars, with main sequence (MS) mass from about $8 - 20$ $M_\odot$. The iron core of a main sequence star is supported by electron degeneracy pressure. The degeneracy pressure can only support a core mass up to the Chandrasekhar mass, $m_{\rm Ch} = 1.4$ $M_\odot$, and the core collapses once its mass surpasses $m_{\rm Ch}$. Stars with masses less than 20 $M_\odot$ also have low enough masses for the core collapse to be halted by neutron degeneracy pressure, resulting in a core collapse supernova which leaves a neutron star as a remnant. A small asymmetry in the supernova gives the newly born neutron star a natal kick.

A binary of two neutron stars is required for two to merge and produce a SGRB. The most obvious production of such a supernova would be a primordial double neutron star binary, where two stars with appropriate masses are simply formed in a binary. A dynamical origin in globular clusters has also been proposed (e.g. Davies 1995), but is not

considered in this paper.

Tauris et al. (2017) show the evolutionary scenario in which a double neutron star binary is formed from a binary of two main sequence stars. The more massive of the two stars, m_2 goes into its giant phase. The binary must be tight enough that Roche lobe overflow occurs, and the less massive m_1 accretes the hydrogen envelope of m_1, leaving m_2 a helium star. m_2 eventually undergoes core-collapse and explodes in a supernova, leaving the first neutron star. If the binary survives, m_1 eventually also enters the giant phase and Roche lobe overflow occurs again. This time, the configuration is dynamically unstable and the binary enters into a common envelope phase where the neutron star of m_2 and helium core of m_1 share a common hydrogen envelope. Dynamical friction shrinks and circularizes the orbit: combined with stellar winds, the dynamical friction also throws out the hydrogen envelope. Left is the neutron star m_2 and naked helium star m_1. m_1 will with time also undergo core collapse, forming the second neutron star in the binary. If the binary remains bound after the second supernova, there are two compact objects orbiting each other in a tight binary. They will emit gravitational radiation, carrying away energy and angular momentum. As a result the binary gradually shrinks until the neutron stars eventually merge.

In this paper, we attempt to find what inputs into the final stages of the double neutron star binary evolution produce SGRBs consistent with the observed distribution of SGRB offsets. In order to do this, we produce a model for the dynamical effects of the formation of the second neutron star in the binary. We then integrate the path of the binary as it traverses its host galaxy, and compare the resulting offsets to the observed population of SGRBs.

Chapter 2

Kick model

We are to develop a model for how the neutron star natal kick affects the double neutron star binary. First, let us describe the binary system at the start of our model. At this point, the binary consists of a naked helium star (with mass $m_{1,\mathrm{i}}$) and a neutron star (with mass $m_2 = 1.4\ \mathrm{M}_\odot$) on a tight circular orbit, as depicted in figure 2.1. We use the notation that x_i denotes initial, that is pre-supernova, quantities of parameter x that change after the supernova – no subscript means that the quantity either does not change or is post-supernova.

In the binary we have an inertial frame in the center of mass

$$M_{\mathrm{i}}\vec{v}_{\mathrm{com,i}} = m_{1,\mathrm{i}}\vec{v}_{1,\mathrm{i}} + m_2\vec{v}_{2,\mathrm{i}} \equiv 0 \tag{2.1}$$

where $M = m_1 + m_2$, $\vec{v}_{j,i}$ is the velocity of star j. We define that the system velocity is initially $\vec{v}_{\mathrm{com,i}} = 0$ – the binary is initially stationary in its inertial frame. Note that we are thus neglecting the history of the binary here, in particular the velocity imparted by the first supernova. We justify this by the much higher total mass of the system after the first supernova. At that point, the binary contained a massive MS star – compared to the two neutron stars comprising the system after the second supernova.

Now, let us assume the supernova explosion occurs instantaneously and isotropically. I.e, the only thing that occurs at first instance is that the exploding helium star loses mass:

$$m_1 = m_{1,\mathrm{i}} - \delta m = 1.4\ \mathrm{M}_\odot$$

Of course, this does impart an impulse on the system. The binary has lost mass and thus momentum, and is effectively kicked in the direction of $-\vec{v}_{1,i}$.

However, we know that an isotropic mass loss is a poor model; we observe that isolated neutron stars receive natal kicks (Lai et al. 2001). We will incorporate this in the simplest way possible, and directly give the exploding star an extra kick velocity $\vec{v}_{\mathrm{k}}$ after the mass loss. Let us express the new binary system velocity:

$$\begin{aligned} M\vec{v}_{\mathrm{com}} = (m_{1,\mathrm{i}} - \delta m)(\vec{v}_{1,i} + \vec{v}_{\mathrm{k}}) + m_2\vec{v}_{2,\mathrm{i}} &= m_1\vec{v}_{\mathrm{k}} - \delta m\vec{v}_{1,\mathrm{i}} + M_{\mathrm{i}}\vec{v}_{\mathrm{com,i}} \\ &= m_1\vec{v}_{\mathrm{k}} - \delta m\vec{v}_{1,\mathrm{i}} \end{aligned} \tag{2.2}$$

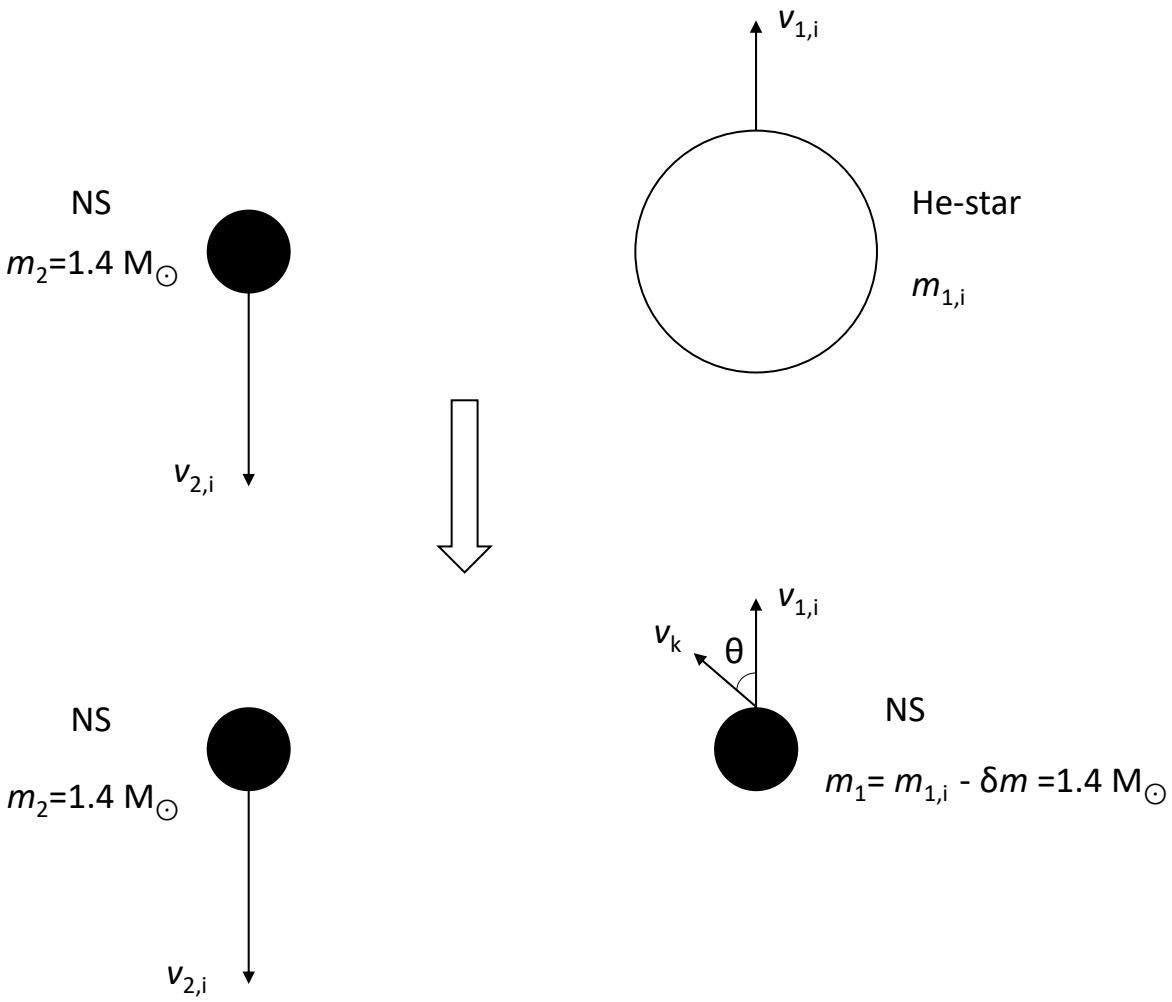

Figure 2.1: Depiction of how we model the second supernova in a double neutron star binary. A NS (m_2) and a He-star ($m_{1,\mathrm{i}}$) are initially on a tight circular orbit, separated by the semimajor axis a_i. In the supernova, the He-star instantaneously loses an amount of mass δm, and is given a natal kick $\vec{v}_\mathrm{k}$. Also shown is the azimuthal angle θ between $\vec{v}_\mathrm{k}$ and $\vec{v}_{1,\mathrm{i}}$ in the plane of the orbit; not shown is the polar angle φ between $\vec{v}_\mathrm{k}$ and said plane.

To reiterate, we model two effects on the velocity of the binary: The impulse imparted by the instantaneous mass loss of the exploding component, and a correction for our assumption of isotropic mass loss.

We have now found one of the parameters we will need in order to find a future position of our binary: the system velocity $\vec{v}_{com}$. However, this velocity is only relevant if the binary in fact remains a binary; we need to know whether the binary remains bound after the supernova. In order to find if the binary remains bound or not, we calculate the energy E of the system. If $E < 0$, it is bound – it is not bound if $E > 0$. In order to calculate the total energy we simply sum the kinetic and potential energies

$$E = \frac{1}{2}(m_1 v_1^2 + m_2 v_2^2) - \frac{G m_1 m_2}{a_\mathrm{i}} \tag{2.3}$$

There are two things to note here. First is that we need to use the velocities of the component stars in the new inertial rest frame of the binary. These are

$$v_1 = |\vec{v}_{1,\mathrm{i}} + \vec{v}_\mathrm{k} - \vec{v}_\mathrm{com}| \quad \& \quad v_2 = |\vec{v}_2 - \vec{v}_\mathrm{com}| \tag{2.4}$$

Second is that we find the potential and kinetic energies at the moment after the instantaneous explosion. That is why we can use the newly found rest frame velocities and initial separation, even though the velocities and separation will change with time.

We are now able to find which systems would be able to survive the supernova. We can thus pose a question: Which systems would survive, if there is no kick? Or, in other words, how massive could we make $m_{1,\mathrm{i}}$ before we start to expect that the system is unlikely to remain bound? We find that

$$E < 0 \Leftrightarrow \delta m < \frac{m_1 + m_1}{2} \tag{2.5}$$

Eq. 2.5 only holds for no kick, as mentioned. The nature of the kick, both its strength and direction, will have an impact on whether the binary remains bound or not. In particular, it affects v_1 in (2.3). If the kick is strong enough, the system will receive enough energy that it will not remain bound. More interesting are weak and moderately strong kicks, where the binary may or may not remain bound depending on the kick direction. Figure 2.2 shows just how the direction of a kick with strength $v_{1,\mathrm{i}}$ affects the system with $m_{1,\mathrm{i}} = 4.2\ \mathrm{M}_\odot$ – where $E = 0$ when no kick is given.

We can see an interesting feature of our kick model in figure 2.2. The most bound systems are the ones with kicks in the $-\vec{v}_{1,\mathrm{i}}$-direction, which is also the direction that the momentum kick from the mass loss imparts on the binary. This means that binaries which receive kicks strong enough to potentially unbind them, will remain bound if the natal kick aligns with the velocity imparted by the mass loss. Thus, for a given binary and kick strength, the binaries which remain bound receive larger system velocities than those which are unbound. Point being, there is a bias towards large velocities for binaries which remain bound.

We have made a model for producing a (possibly surviving) double neutron star binary, that has received some system velocity. As the two neutron stars circle each other, they

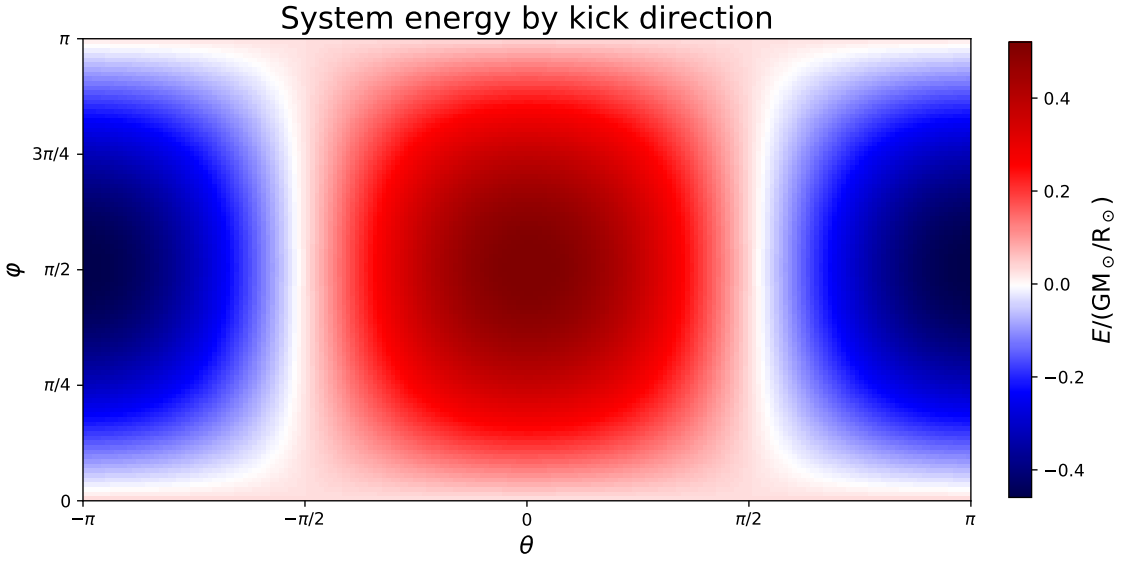

Figure 2.2: Resulting system energy E as simulated in the model. A kick $v_{\mathrm{k}} = v_{1,\mathrm{i}}$ is given while varying kick direction, in a system with $m_{1,\mathrm{i}} = 4.2\ M_\odot$. θ and φ define the angle between $\vec{v}_{\mathrm{k}}$ and $\vec{v}_{1,\mathrm{i}}$, as described in figure 2.1. $(\theta, \varphi) = (0, \pi/2)$ means $\vec{v}_{\mathrm{k}} \parallel \vec{v}_{1,\mathrm{i}}$, while $(\theta, \varphi) = (\pi, \pi/2)$ means $\vec{v}_{\mathrm{k}} \parallel -\vec{v}_{1,\mathrm{i}}$

will emit gravitational waves that carry away energy and angular momentum (Taylor & Weisberg 1982). As a result, the binaries start to inspiral. When the binary components grow closer the gravitational wave emission grows stronger, meaning there is a strong feedback loop. The result is that double neutron star binaries have a finite lifetime before the neutron stars merge. An approximation of this merger time τ is given by Lorimer (2008).

$$\tau \approx 9.83 \cdot 10^6 \text{ yr} \left(\frac{P_{\mathrm{b}}}{\mathrm{hr}}\right)^{8/3} \left(\frac{m_1 + m_2}{\mathrm{M}_\odot}\right)^{-2/3} \left(\frac{\mu}{\mathrm{M}_\odot}\right)^{-1} \left(1 - e^2\right)^{7/2} \tag{2.6}$$

Here, P_{b} is the orbital period of the binary, $\mu = \frac{m_1 m_2}{m_1 + m_2}$ the reduced mass of the system, and e the orbital eccentricity. We have plotted isochromes of τ in a-e space in figure 2.3 to illustrate how changes in orbital period and eccentricity lead to very different merger times.

The next step is obviously to find the two parameters in (2.6) which we have not already found - P_{b} and e. We start with the orbital period, by finding the semimajor axis of the system. We know that the semimajor axis is related to the potential energy U of the system, and that the total energy in the two body problem is half the potential energy:

$$\begin{aligned} E = \frac{1}{2}U = -\frac{1}{2}\frac{Gm_1m_2}{a} \\ \Rightarrow \quad a = -\frac{Gm_1m_2}{2E} \end{aligned} \tag{2.7}$$

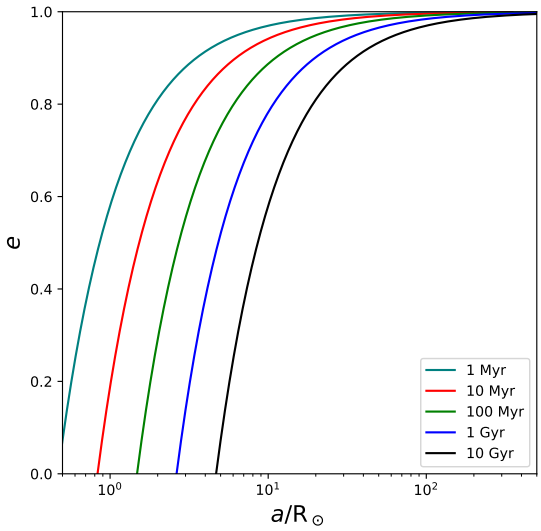

Figure 2.3: Isochromes of merger time τ in a-e space.

Then we simply use Kepler's third law to obtain the period.

$$P_{\rm b} = \frac{2\pi a^{3/2}}{\sqrt{G(m_1 + m_2)}} \tag{2.8}$$

Meanwhile, the angular momentum J of an elliptical orbit can be found by correcting the circular angular momentum J_c by the orbital eccentricity

$$J = J_{\rm c}\sqrt{1 - e^2} \tag{2.9}$$

where $J_{\rm c}$ is

$$J_{\rm c} = \mu\sqrt{GMa} \tag{2.10}$$

J is also defined as

$$J \equiv \left| \sum_{\rm j} m_{\rm j} \vec{r}_{\rm j} \times \vec{v}_{\rm j} \right| \tag{2.11}$$

so we can solve for e in (2.9)

$$e = \sqrt{1 - \left(\frac{J}{J_{\rm c}}\right)^2} \tag{2.12}$$

We have now found all we need in our kick model to produce a distribution of SGRB offsets – the system velocity $v_{\rm com}$ the binary receives, whether it remains bound as well as the time it takes for the binary to merge.

Chapter 3

Population synthesis

To produce a population of SGRB, we need a population of initial binaries to use our kick model upon. I.e, we need an initial distribution of masses $m_{1,\mathrm{i}}$, semimajor axes a_{i}, and natal kicks $\vec{v}_{\mathrm{k}}$.

We expect that helium stars of mass $2-8$ $\mathrm{M}_{\odot}$ will produce neutron stars in isolation (Hurley et al. 2000). In a binary there is the possibility for the helium star to lose mass by mass transfer to its companion, while still collapsing into a neutron star – as discussed in the introduction. We take a conservatively large range for $m_{1,\mathrm{i}}$, between $1.5-8$ $\mathrm{M}_{\odot}$.

To obtain the distribution of masses, we use the main sequence initial mass function (IMF) and interpolate to the appropriate helium star mass. We use the Salpeter IMF (Salpeter 1955)

$$\frac{dN}{dm_{\mathrm{MS}}} \propto m_{\mathrm{MS}}^{-2.35} \tag{3.1}$$

which we assume to be constant throughout the history of the host galaxy for all masses. To interpolate from the main sequence mass to helium star mass we follow the approximation in Davies et al. (2002):

$$m_{\mathrm{He}}\left(m_{\mathrm{MS}}\right) \approx 0.125 m_{\mathrm{MS}}^{1.4} \tag{3.2}$$

We know that tight binaries are produced by the common envelope evolution. As a rough approximation to the results of common envelope evolution, we use an inverse (a_{i}^{-1}) distribution. We put an ad hoc upper limit of 215/2 $\mathrm{R}_{\odot}$ (i.e. about half an AU) to this distribution. Later in this paper we show that this limit is justified, as the binaries must be tighter for a noticeable fraction of them to merge within Hubble time and produce the SGRBs we are interested in.

The lower limit to the semimajor axis can be justified on physical grounds, however. The stars cannot be so close to each other that mass transfer occurs, changing the initial mass parameter. Mass transfer occurs when the helium star exceeds the extent of the Roche lobe, and the Roche lobe depends on the separation of the binary. We follow the approximation in Eggleton (1983), where the Roche lobe is approximated as a sphere with radius

$$r_{\mathrm{L}} = \frac{0.49 q^{2/3}}{0.6 q^{2/3} + \ln\left(1+q^{1/3}\right)} a = f(q) a \tag{3.3}$$

where q is the mass fraction $m_{1,\mathrm{i}}/m_2$. I.e, we approximate that mass transfer occurs when the radius R of $m_{1,\mathrm{i}}$ is larger than r_{L}. Hence, we also need to find the radius of a helium star, which we do in Hurley et al. (2000).

$$R = \frac{0.2391 m_{1,\mathrm{i}}^{4.6}}{m_{1,\mathrm{i}}^4 + 0.162 m_{1,\mathrm{i}}^3 + 0.0065} \tag{3.4}$$

To find the lower limit $a_{\min}$ of the semimajor axis we simply consider

$$\begin{aligned} R = r_{\mathrm{L}} &= f(q) a_{\min} \\ \Leftrightarrow \quad a_{\min} &= \frac{R}{f(q)} \end{aligned} \tag{3.5}$$

Our final free parameter is the kick $\vec{v}_{\mathrm{k}}$. Hobbs et al. (2005) derives a kick distribution from observing the proper motion of local neutron stars, assuming isotropic distribution. The derived distribution is a Maxwellian

$$P(v) = \frac{\pi}{2\left(\frac{\pi}{2}\sigma_{1\mathrm{D}}^2\right)^{3/2}} v^2 \mathrm{e}^{-\frac{v^2}{2\sigma_{1\mathrm{D}}^2}} \tag{3.6}$$

with $\sigma_{1\mathrm{D}} = 265$ km/s. As this was derived assuming isotropic distribution, we also distribute the kick directions isotropically.

There are two underlying assumptions that should be noted here. The first is that this distribution was derived for local, observable, neutron stars – i.e. pulsars in the Milky Way that are young enough that their high frequency radio pulses can still be observed. In other words, eq. (3.6) was derived from a stellar population with the chemical composition of stars currently formed in the Milky Way. Neutron stars can remain in a binary orbit for billions of years before they merge, and therefore may have a very different chemical composition – and hence also may have different kick distributions.

The second assumption is that we can use kicks derived from isolated neutron stars for core-collapse supernovae in binaries. E.g Tauris et al. (2017) proposes an evolutionary scenario where the helium star is stripped of most of its outer layers. They further point out that this would result in much weaker kicks, on the order of tens of km/s.

Results of population synthesis

We now have everything that is needed to produce a number of binaries, where we know whether or not the binary survives, the total system velocity the binary receives from the supernova, and when the binary will merge. Let us now investigate the model, starting with the relation between kick velocity v_{k} and system velocity v_{com}. This relation is presented in figure 3.1 for a few different $m_{1,\mathrm{i}}$ and a_{i} when the system receives different kicks in random directions.

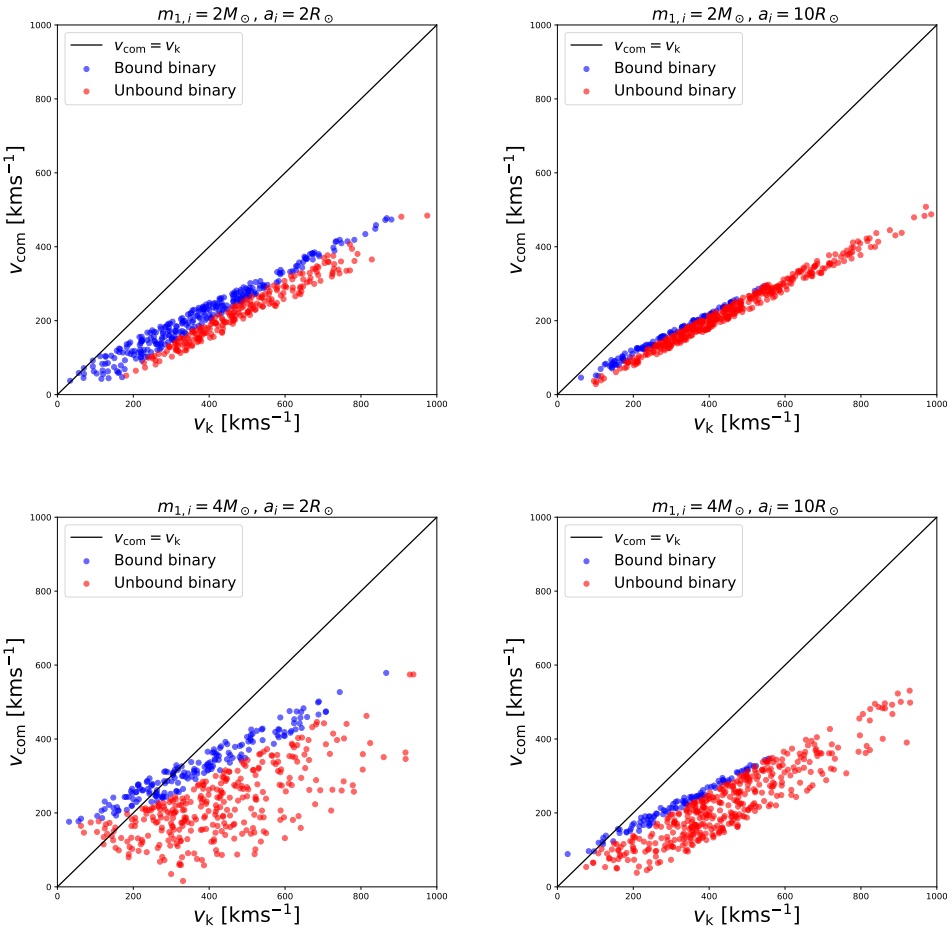

Figure 3.1: Shown are the kick velocity $v_{\rm k}$ and resultant system velocity $v_{\rm com}$ for 500 binaries generated in our model, for different constants $a_{\rm i}$ and $m_{1,\rm i}$ while giving a random kick direction.

In figure 3.1 we can see that the systems which remain bound are indeed the systems which receive a larger system velocity for a given kick. We can also see a qualitative difference between the systems in that the more massive systems can receive a system velocity larger than the kick velocity, while the less massive ones do not. The reason why can be found by considering (2.2): there is a larger mass difference δm so there is already a significant velocity contribution from the mass loss, even before a kick is imparted.

Similarly, the low-a_i systems also have larger velocities when a kick is absent, most clear in the 4 $\mathrm{M}_\odot$ systems. Again, the reason why can be seen in (2.2). The velocity of a body on a circular Keplerian orbit has a proportionality to its semimajor axis as $v \propto a^{-1/2}$. Hence, $v_{1,\mathrm{i}}$ is larger for tighter systems and the momentum imparted on the system from the mass loss larger.

Let us now consider a more central question. For which part of the parameter space of $m_{1,\mathrm{i}}$ and a_i can we expect that a binary will survive the supernova? What is the fraction of systems which are bound given $m_{1,\mathrm{i}}$ and a_i? We can make some preliminary predictions of the behaviour of the bound fraction. The larger the initial semimajor axis, the smaller the initial binding energy of the binary – larger initial semimajor axes should have a smaller bound fraction. Similarly, a larger initial mass means that more energy is given to the system from the larger momentum kick of the mass loss – larger initial masses should also have a smaller bound fraction.

However, we can also quantify the bound fraction theoretically. First, consider the bound condition of the binary in the reduced mass formalism:

$$E = \frac{1}{2}\mu v_\mathrm{b}^2 - \frac{G m_1 m_2}{a_\mathrm{i}} = 0 \quad \Rightarrow \quad v_\mathrm{b}^2 = \frac{2G(m_1+m_2)}{a_\mathrm{i}} \tag{3.7}$$

We are saying that if the relative velocity v_r is less than the critical velocity v_b, i.e. if $v_\mathrm{r} < v_\mathrm{b}$, the system is bound. The relative velocity is frame invariant – so we can put ourselves in the frame of m_2. In this frame, m_1 has a velocity

$$v_\mathrm{c}^2 = \frac{G m_{1,\mathrm{i}} m_2}{a_\mathrm{i}} \tag{3.8}$$

before the supernova. After the supernova it has a new relative velocity

$$v_\mathrm{r}^2 = \left[v_\mathrm{c} + v_\mathrm{k}\cos(\Theta)\right]^2 + \left[v_\mathrm{k}\sin(\Theta)\right]^2 = v_\mathrm{c}^2 + v_\mathrm{k}^2 + 2v_\mathrm{c}v_\mathrm{k}\cos(\Theta) \tag{3.9}$$

where Θ is the angle between $\vec{v}_\mathrm{c}$ and the kick $\vec{v}_\mathrm{k}$. The normalized integral over all possible v_k and Θ (i.e, all possible kicks) is

$$\int_0^\pi \int_0^\infty \frac{1}{2}\sin(\Theta) P(v_\mathrm{k}) dv_\mathrm{k} d\Theta = 1 \tag{3.10}$$

If we would only count the systems which end up bound, we receive the bound fraction. So let us only count the bound systems by introducing

$$H(v_\mathrm{r}^2 - v_\mathrm{b}^2) = \begin{cases} 1 & \text{if } v_\mathrm{r}^2 - v_\mathrm{b}^2 < 0 \\ 0 & \text{if } v_\mathrm{r}^2 - v_\mathrm{b}^2 \geq 0 \end{cases} \tag{3.11}$$

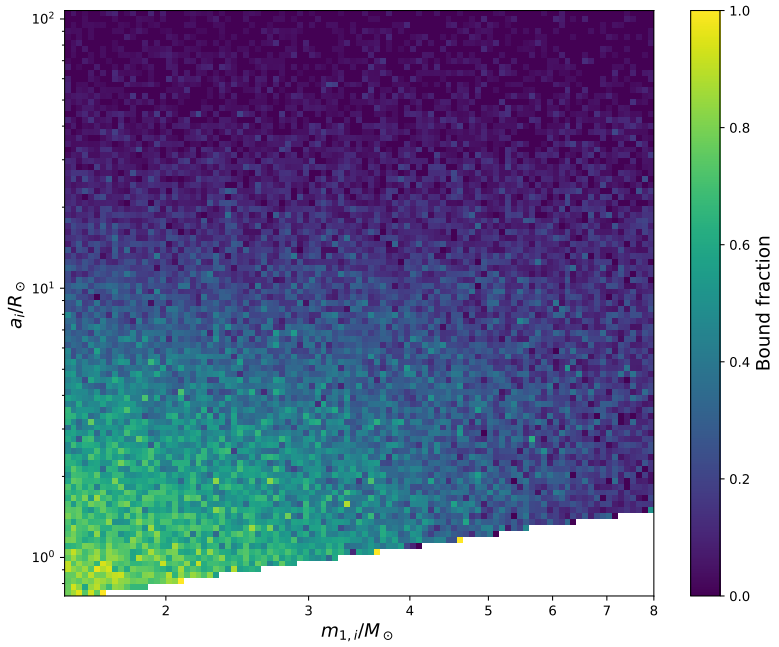

Figure 3.2: Fraction of bound systems generated in the model allocated over 100×100 bins of initial semimajor axis a_i and mass $m_{1,\mathrm{i}}$. 250,000 binaries generated in total.

to the integrand:

$$P_{bound} = \int_0^\pi \int_0^\infty \frac{1}{2} \sin(\Theta) P(v_\mathrm{k}) H(v_\mathrm{r}^2 - v_\mathrm{b}^2) dv_\mathrm{k} d\Theta \tag{3.12}$$

The resulting bound fraction from running the model can be seen in figure 3.2. Comparing the values computed numerically from the theoretical expression in (3.12) confirms that they indeed produce the same results, which also agree with our preliminary prediction. Note also the "forbidden" region in lower part of the plot. It is the part of parameter space where the semimajor axis a_i results in a Roche lobe $r_\mathrm{L} > R$ for the given mass.

We are still interested in the system velocity of the binaries which remain bound. We can confidently predict the general behaviour beforehand, as there is a straightforward relation from a_i and $m_{1,\mathrm{i}}$. If a_i is low $v_{1,\mathrm{i}}$ is high and if $m_{1,\mathrm{i}}$ is high δm is high. Looking back to (2.2) we see that a low a_i and high $m_{1,\mathrm{i}}$ favours high system velocities. Looking at the average system velocities generated in the model in figure 3.3 confirms this. Note that system velocities of about 200 km/s are reached for tight low mass binaries (see figure 3.3). We will later argue that system velocities of this strength are key to the distribution of SGRB.

The merger time of the binaries which remain bound is also of interest, to be able to find where they merge. The general behaviour is much less straightforward here. However,

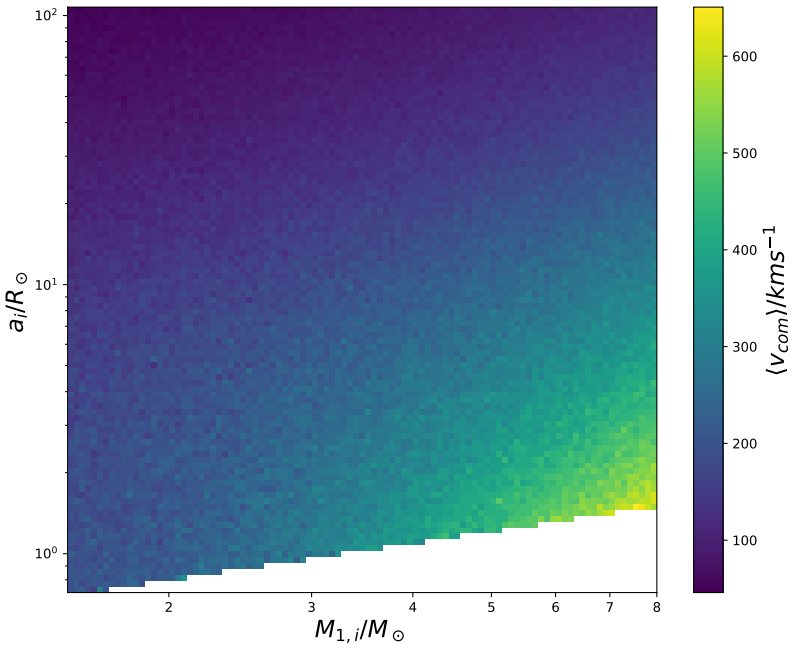

Figure 3.3: Average system velocity $v_{\rm com}$ of bound systems generated in the model allocated over 100×100 bins of initial semimajor axis $a_{\rm i}$ and mass $m_{1,{\rm i}}$. 250,000 bound binaries generated in total.

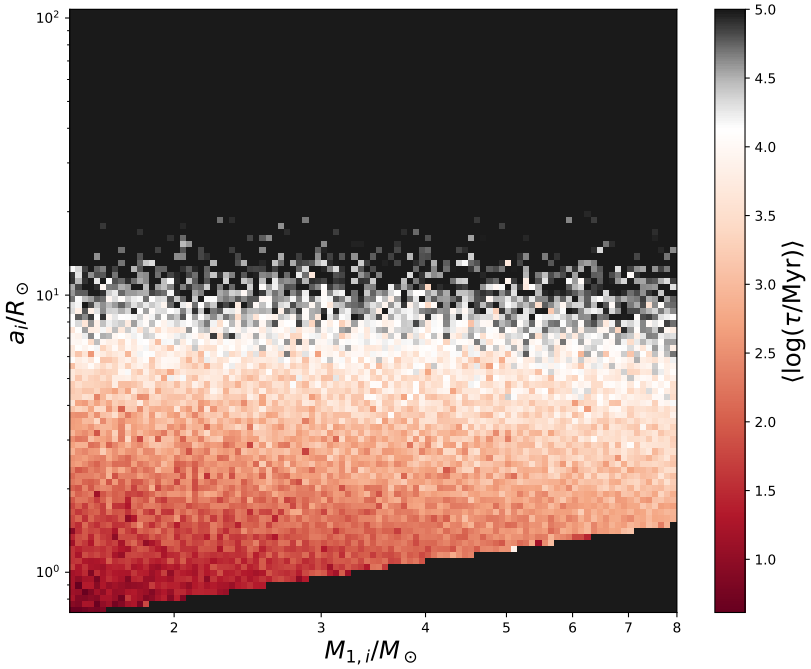

Figure 3.4: Average of merger time $\log \tau$ for bound systems generated in the model allocated over 100×100 bins of initial semimajor axis a_i and mass $m_{1,\mathrm{i}}$. 250,000 bound binaries generated in total. All bins with $\langle \log(\tau/\mathrm{Myr}) \rangle > 5$ set to black, to show which part of parameter space represents binaries that do not merge within Hubble time.

τ has a very strong dependence on a as seen in (2.6). The binaries that start wide will most likely also end up comparatively wide after the supernova, and therefore have longer merger times. Furthermore, for a given a_i, a low mass binary will most likely end up more bound than a large mass binary – and therefore have a smaller a. Low mass binaries should hence also favour short merger times. The actual distribution generated in the model can be seen in figure 3.4.

The histogram in figure 3.4 shows just how strong the dependence of τ on a_i is. We can neglect the majority of the phase space which we are probing, as systems with $a_\mathrm{i} \gtrsim 20$ $\mathrm{R}_\odot$ only merge after 100 Gyr on average – far greater than the Hubble time. Furthermore, we also saw in figure 3.2 that such wide systems are also unlikely to remain bound. In contrast, $\langle \log(\tau/\mathrm{Myr}) \rangle$ is much less dependent on $m_{1,\mathrm{i}}$, although τ still spans several orders of magnitude for a given a_i.

We claim that the majority of investigated semimajor axes are unlikely to provide binaries that merge within Hubble time, and thus are not of interest. To justify this, we need to look more deeply into the distribution of τ for a large a_i. It is conceivable that a significant portion of binaries actually merge within Hubble time for the given large a_i,

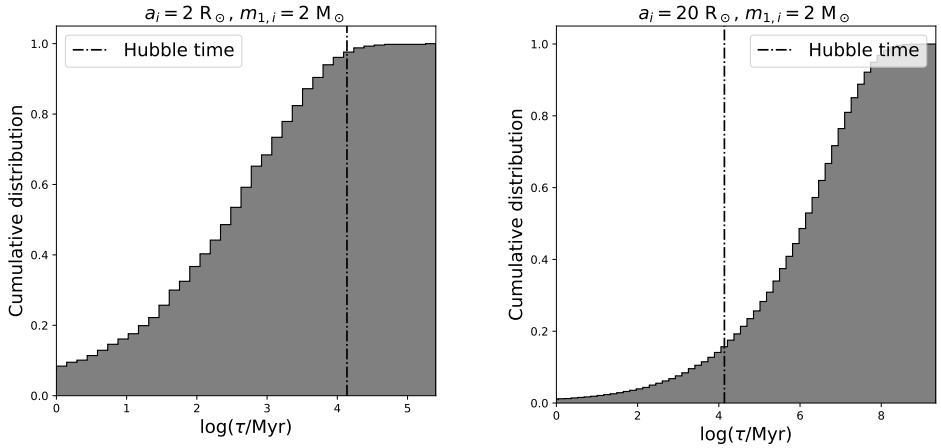

Figure 3.5: Shown here, the cumulative distribution of merger times for two different sets of initial parameters while varying kick strength and direction. On the left, $a_\mathrm{i} = 2\ \mathrm{R}_\odot$ and $m_{1,\mathrm{i}} = 2\ \mathrm{M}_\odot$. On the right, $a_\mathrm{i} = 20\ \mathrm{R}_\odot$ and $m_{1,\mathrm{i}} = 2\ \mathrm{M}_\odot$.

even though the average is far greater. The right plot of figure 3.5 shows that $\sim 15\%$ of systems with a conservative $a_\mathrm{i} = 20$ and $m_{1,\mathrm{i}} = 2$ merge within Hubble time. Still, only $\sim 10\%$ of binaries with said initial parameters survive the supernova in the first place – both these numbers are less for systems with higher a_i.

In a similar vein, the left plot of figure 3.5 shows the cumulative distribution for a tight, low mass system. Here, we see that the majority of systems merge between a Myr and a few Gyr. Let us show why the relevant time scale is within this range, given that SGRB are observed at offsets up to a few tens of kpc.

Figure 3.6 shows how binaries generated in the model are scattered over system velocities and merger times. Also shown are several isodistance lines. These isodistance lines show the maximal distance a binary could possibly travel before they merge, demonstrating what time scales are relevant for an observed high-offset SGRB. To find the actual trajectory of one of the binaries is more complicated, however.

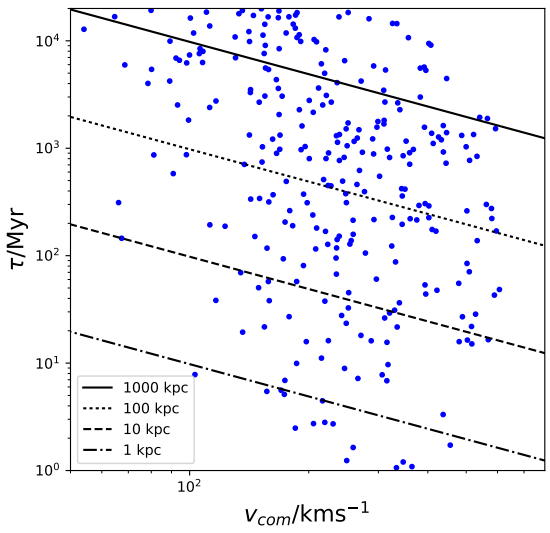

Figure 3.6: Scatter of 250 binaries produced in the model for system velocity and merger times. Also shown are four isodistance lines where $v_{\rm com} \cdot \tau = 1$ kpc, 10 kpc, 100 kpc, and 1000 kpc.

Chapter 4

Host galaxies

So far, we have made a model in which we can find the system velocity a binary will receive from the supernova explosion, and how long it lives until it merges. To find its trajectory we also need to know the dynamics of the galactic environment it is travelling in: we need to know the potential of the host galaxy. We use the simplest type of potential, a spherically symmetric potential. Specifically, we adopt the potential Φ arising from a density profile given in Thomas et al. (2009)

$$\rho = \frac{v_{\rm h}^2}{4\pi G} \frac{3r_{\rm h}^2 + r^2}{\left(r_{\rm h}^2 + r^2\right)^2} \tag{4.1}$$

which yields the logarithmic potential

$$\Phi = \frac{v_{\rm h}^2}{2} \ln\left(r_{\rm h}^2 + r^2\right) \tag{4.2}$$

where r is the distance from the center of the galaxy, $r_{\rm h}$ the scale radius of the galactic dark matter halo, and $v_{\rm h}$ the circular velocity which is asymptotically approached at large r.

We have now defined the environment of the binary. What is left before we can integrate over the potential and find the offset of the SGRB is defining the initial conditions of the binary: where was it and what velocity did it have before the supernova?

We place the binaries in an exponential disc, i.e according to

$$2\pi r \mathrm{e}^{-r/r_{\rm e}} \tag{4.3}$$

where $r_{\rm e}$ is the radius of the baryonic matter of the galaxy. Note that we place the binaries in a disc, i.e. in a spiral galaxy. This is done intentionally; we do not aim to take into account the dynamical and star formation histories of elliptical galaxies in this paper.

As for the initial velocity v_i, we approximate initially circular orbits. I.e,

$$v_i^2 = \frac{-\nabla\Phi}{r} \tag{4.4}$$

$v_{\rm com}$	ϵ
0 $\rm kms^{-1}$	$3.2 \cdot 10^{-12}$
20 $\rm kms^{-1}$	$6.1 \cdot 10^{-12}$
200 $\rm kms^{-1}$	$3.3 \cdot 10^{-10}$
500 $\rm kms^{-1}$	$2.5 \cdot 10^{-9}$

$v_{\rm com}$	ϵ
0 $\rm kms^{-1}$	$2.4 \cdot 10^{-5}$
20 $\rm kms^{-1}$	$3.2 \cdot 10^{-5}$
200 $\rm kms^{-1}$	$7.2 \cdot 10^{-5}$
500 $\rm kms^{-1}$	$1.3 \cdot 10^{-4}$

Table 4.1: The maximal fractional energy error $\max(\epsilon)$ of our integrator as we calculate the trajectory of a particle through a test galaxy, while giving different kicks $v_{\rm com}$. On the left, as we integrate over 1 Gyr with a timestep of 1 Myr. On the right, as we integrate over 14 Gyr with a timestep of 14 Myr.

Galactic integration

The equation of motion for the potential in (4.2) is not analytically solvable. A numerical method to integrate the equation of motion and find the trajectory of a binary is required. We have built and use a fourth order Runge-Kutta integrator. We present the results of our integrator when tested in a hypothetical host galaxy with $r_{\rm h} = 10$ kpc, $v_{\rm h} = 140$ km/s in figure 4.1. The test is performed by putting the test particle on an initially circular orbit and then applying a velocity kick $v_{\rm com}$ in the direction of motion and integrating over one Gyr.

When we later use the integrator we keep the number of timesteps constant at 1000 steps (as used in the integration for figure 4.1), regardless of the length of time we integrate over. To ensure that our integrator is still calculating the correct trajectories, we investigate the fractional energy error ϵ

$$\epsilon = \left(\frac{|\epsilon_{\rm x} - \epsilon_0|}{\epsilon_0} \right) \tag{4.5}$$

where ϵ_0 is the specific energy at the starting position, while $\epsilon_{\rm x}$ is the specific energy at some timestep. ϵ increases in a linear trend over the course of the integration. The maximal fractional energy error, as presented in table 4.1, shows that the error in the integrator never grows large enough to change the final position qualitatively while integrating over Hubble time, however.

GRB/Galaxy population

The point of this paper is to compare the SGRBs produced in our model to observed SGRBs. For that we need a set of observed bursts, which we take from Church et al. (2011). Church et al. (2011) also attribute a host galaxy to the bursts based on least chance probability, as well as predicting the properties of the host. We present the relevant properties of the SGRBs and host galaxies in table 4.2. Where an observed effective radii was not available, the authors took the radius as the half-light radius of the galaxy. Note that the link between the baryonic galaxy matter and dark matter halo used by the authors is based on observations in the local Universe – not necessarily accurate for higher redshifts.

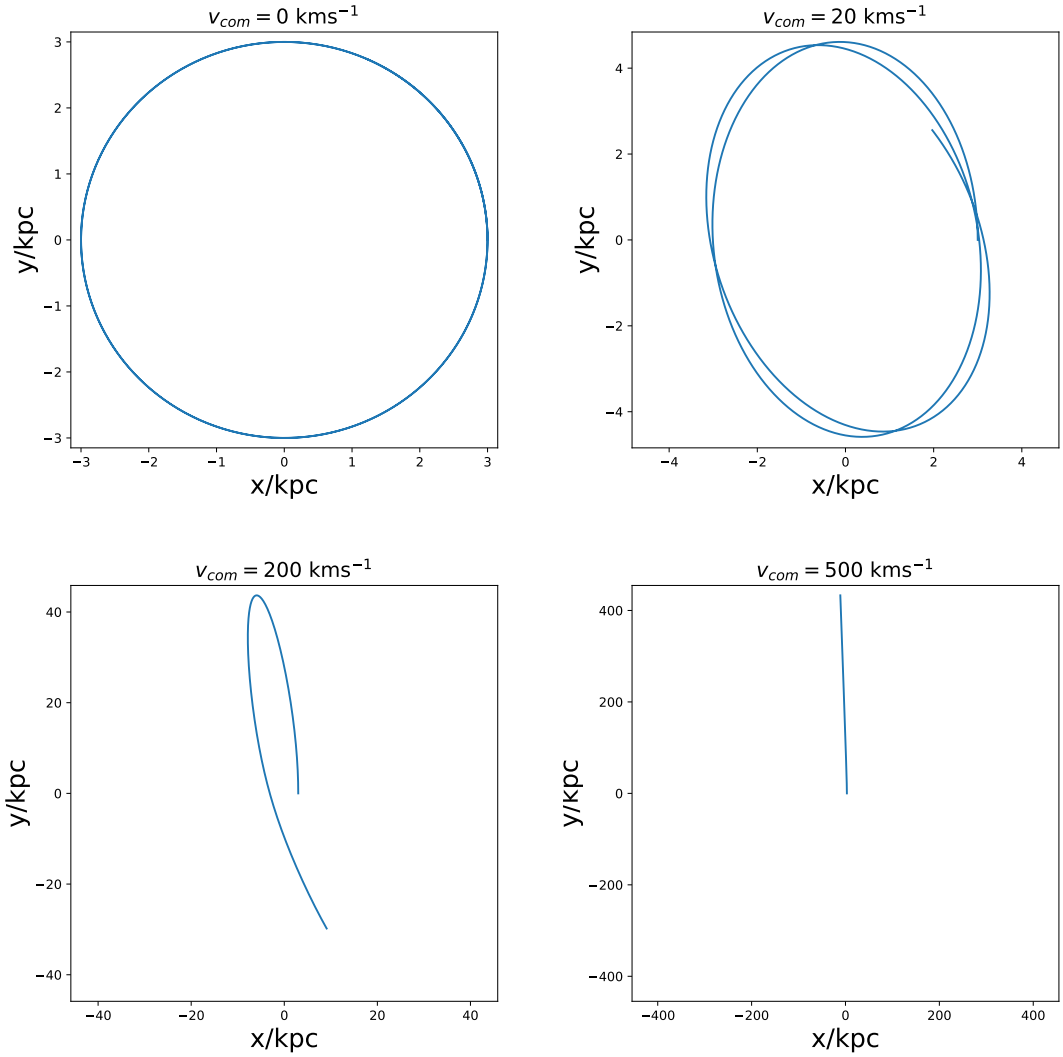

Figure 4.1: Trajectories calculated using our integrator. Test galaxy has $r_{\rm h} = 10$ kpc, $v_{\rm h} = 140$ km/s. Test particle put on a circular orbit, and then given a further $v_{\rm com}$ in direction of motion. Particle trajectory integrated over one Gyr.

GRB	R	$\sigma_{\rm off}$	$r_{\rm e}$	$r_{\rm e}^{\rm obs}$	$r_{\rm h}$	$v_{\rm h}$	z	T
	kpc	kpc	kpc	kpc	kpc	km/s		Gyr
051221A	1.53	0.31	2.42	2.17	15.66	157.30	0.546	8.31
060801	19.7	14.0	3.00		18.20	170.23	1.130	5.41
061006	1.44	0.29	1.26	3.67	9.92	123.65	0.438	9.09
061201	33.9	0.4	1.20	1.80	9.59	121.45	0.111	12.28
061210	10.7	6.9	2.62		16.54	161.88	0.410	9.32
061217	55	20	1.81		12.81	141.48	0.827	6.67
070429B	4.7	4.7	2.10		14.19	149.31	0.902	6.32
070714B	3.08	0.47	0.94		8.90	111.02	0.923	6.23
070809	19.61	1.9	0.92		8.00	110.42	0.219	11.07
071227	16.1	0.2	3.13		18.77	173.00	0.394	9.45
080905A	18.11	0.42	2.98		18.14	169.92	0.122	12.15

Table 4.2: Offsets of the SGRBs investigated, along with details of the host galaxy. By column from the left: burst identifier, measured offset R, one-sigma error $\sigma_{\rm off}$ in the measured offset assuming Gaussian point spread function, predicted radius $r_{\rm e}$ of host galaxy, observed radius $r_{\rm e}^{\rm obs}$ of host galaxy where available, scale radius $r_{\rm h}$ of the host galaxy dark matter halo, asymptotic rotational velocity $v_{\rm h}$ of the host galaxy, redshift z of the host galaxy, and age T of the Universe at the redshift of the host galaxy (Church et al. 2011). T calculated from z according to Wright (2006).

T, the local Hubble time in each host galaxy, was calculated according to Wright (2006) assuming Hubble constant $H_0 = 69.6$ kms^{-1}Mpc^{-1}, ratio of density of the Universe to the critical density $\Omega_{\rm M} = 0.286$ and cosmological constant density $\Omega_\lambda = 0.714$ (Bennett et al. 2014).

Chapter 5

Results

For each of the galaxies in table 4.2 we have produced one million bound binaries. Of these million binaries we kept those with $\tau < T$, i.e. the binaries with lifetimes less than the age of the Universe at the burst redshift. This is an upper approximation to the time the galaxy has been producing stars. We have then integrated the trajectory of the kept binaries until the time they merge. We present the resulting offsets in the xy-plane (parallel to the disc) as well as the xz-plane in figure 5.1, for the galaxy hosts of 060801 and 061201. The galaxies are chosen as the youngest and oldest of our sample, respectively. We expect there to be some difference in the distribution of offsets between the planes, as we initially place the binaries in – and with velocities in – the disc of the xy-plane.

In figure 5.1 we can clearly see that we are able to produce all observed bursts in our model. This means that the Hobbs et al. (2005) natal kick is capable of producing all observed offsets. However, there seems to be a an overrepresentation of large offsets, especially in 061201: here, an offset of > 100 kpc is more likely than one with < 2 kpc. As expected we also see some difference between the offsets in the xy and xz-planes. Low offsets are more probable in the xz-plane and high offsets are equally probable in both planes, consistent with the binaries initially being placed at $z = 0$ with $v_z = 0$.

We have also investigated the binaries which produce bursts consistent with the observed burst for each galaxy. Bursts were chosen according to a Gaussian centered on the observed offset with σ_{off}; these are then compared with the total population of bursts in the galaxy. $m_{1,\text{i}}$-a_{i}, v_{com}-τ, and a-e parameter space were investigated. There is a clear, gradual change between the close and distant bursts; the results for 061006 and 061201 are shown in figures 5.2 and 5.3. 061006 is chosen as the observed GRB with the smallest offset, while 061201 has the second largest offset. GRB 061217, with the largest observed offset, is not chosen to represent the distant bursts. This is due to the large error in the offset, which makes the data less clear and harder to read. Comparison to the rest of the bursts can be found in the appendix, ordered from smallest to largest observed offset.

From figures 5.2 and 5.3 we see that all binaries with $m_{1,\text{i}}$ in the range $1 - 8$ $\text{M}_\odot$ are capable of producing SGRBs with the offsets we observe. Furthermore, as already discussed, binaries separated by more than ~ 20 $\text{R}_\odot$ do not produce bursts due to the combination of long lifetimes and low bound fraction. The produced population of close

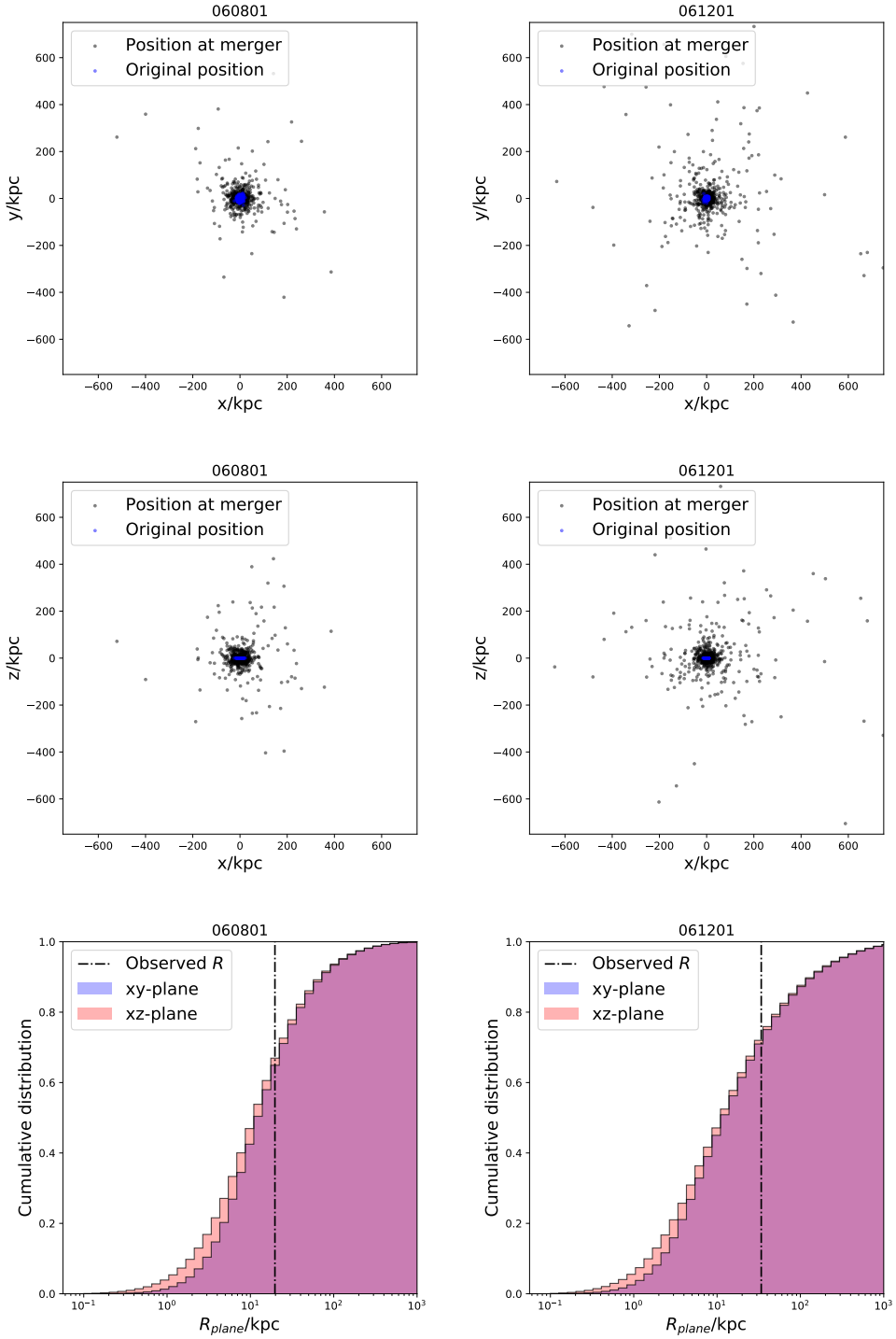

Figure 5.1: First row: Original binary position in blue and position at merger in black, for the xy-plane parallel to the disc of the galaxy. Second row: Same, but for xz-plane. Third row: Histograms of the burst offsets in the planes. Left column for GRB 060801, right column for GRB 061201.

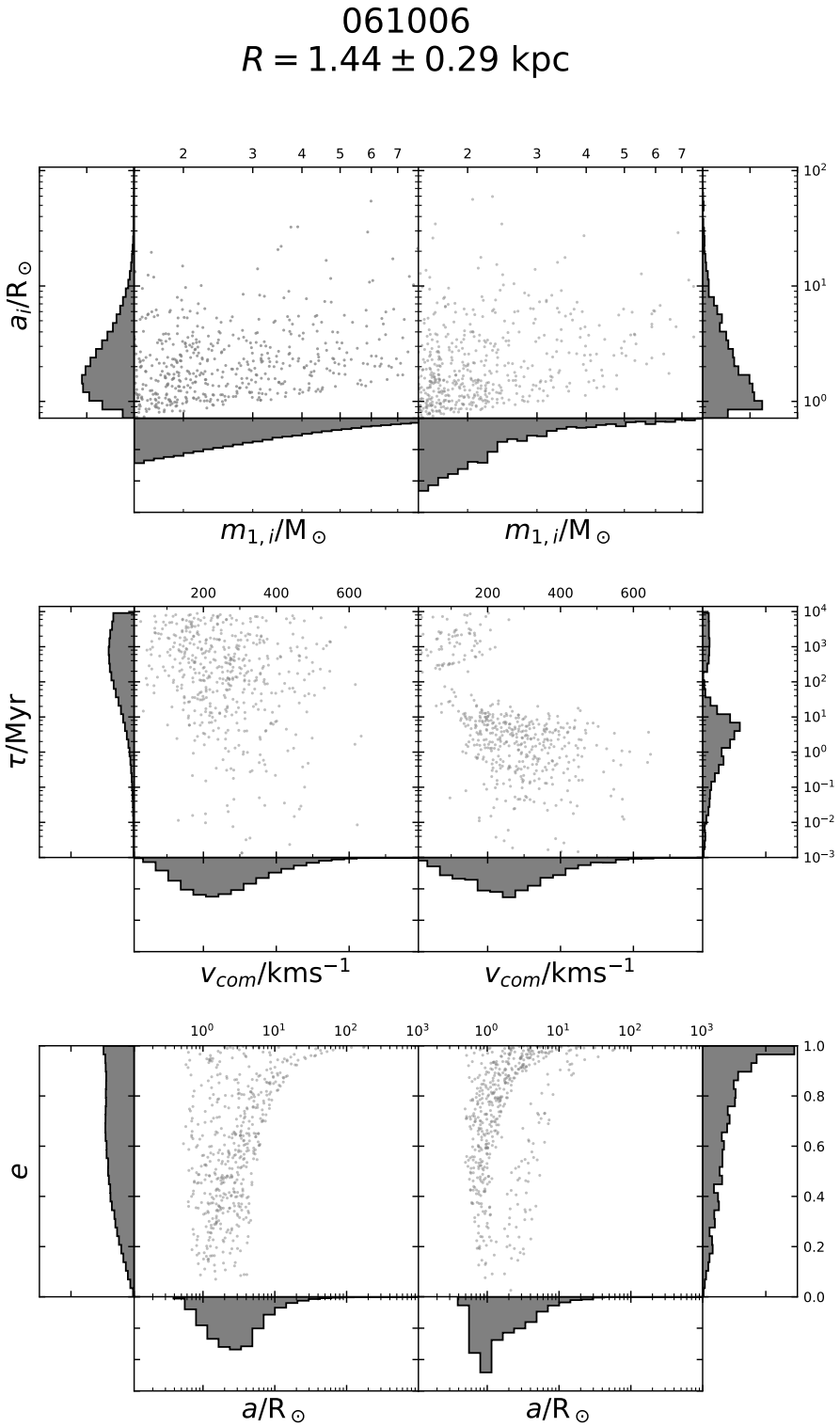

Figure 5.2: Produced bursts in $m_{1,\mathrm{i}}$-a_i, v_com-τ, and a-e space in the host galaxy of 061006. On the left half, bursts generated with $\tau < T$. On the right, bursts are further constrained according to the probability of a Gaussian centered on R with σ_off.

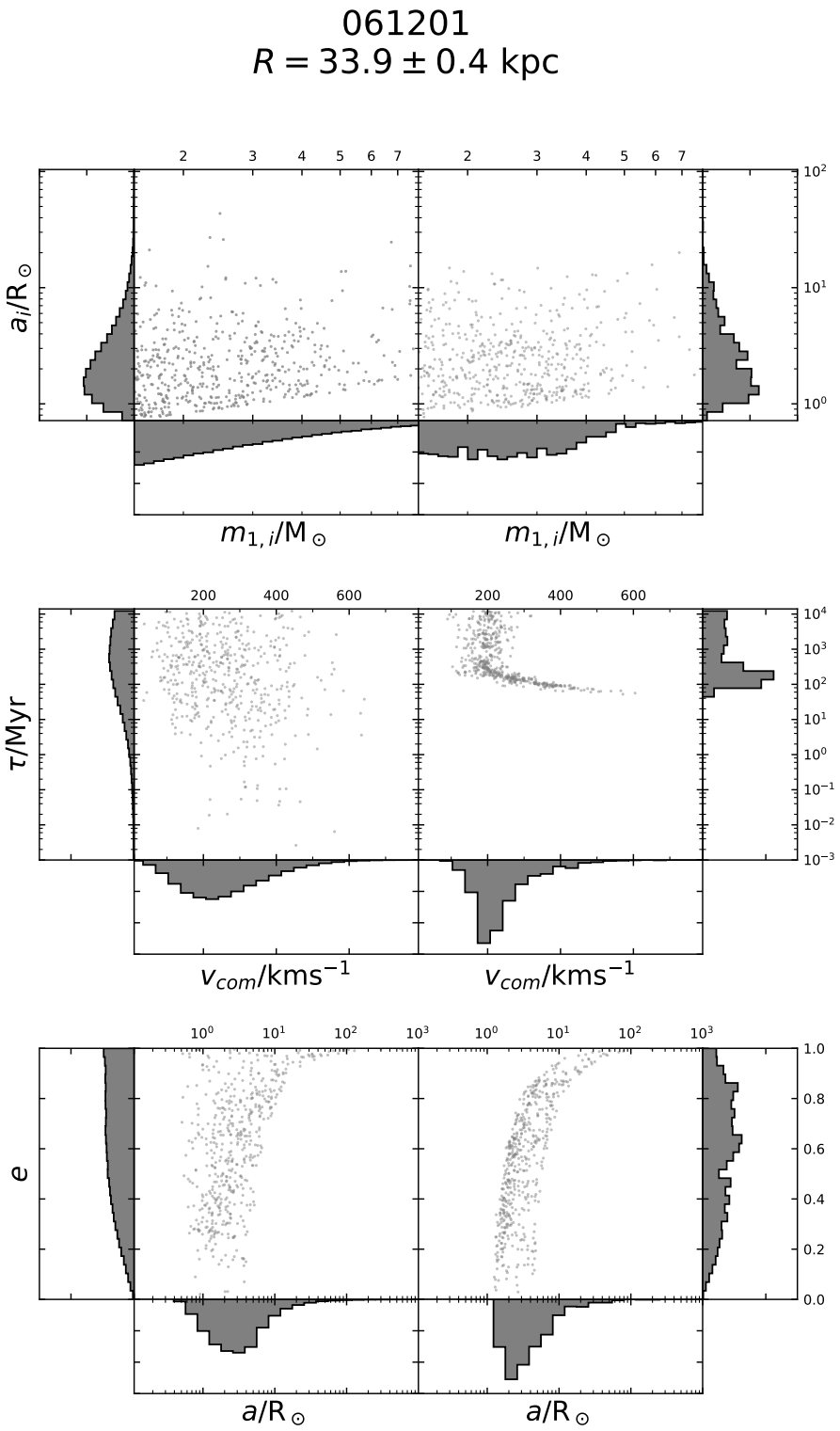

Figure 5.3: Same as figure 5.2, but for GRB 061201.

bursts in figure 5.2 are mainly concentrated at tight binaries and low masses. This is consistent with the majority of these bursts having low lifetimes. In contrast, the observed distant bursts of 061201 (seen in figure 5.3) favour intermediate masses. Again, this is consistent with the distant binaries having exclusively longer lifetimes ($gtrsim$100 Myr) and mainly receiving $v_{\rm com} \approx 200$ km/s (c.f. figures 3.4 and 3.3).

To summarize what see regarding the inputs into the final stages of the evolution of DNS binaries: After the CE evolution, the NS-He-star binary requires a semimajor axis $a_{\rm i}$ greater than ~ 20 $R_\odot$ for the binary to eventually merge within Hubble time; the He-star can have any mass $m_{1,{\rm i}}$ within the range of NS-producing masses; a natal kick $v_{\rm k}$ derived from isolated neutron stars in the Milky Way is more than enough to produce a SGRB at the most distant observed offsets.

Chapter 6

Discussion

We see some distinction between close and distant burst offsets. In the $v_{\rm com}$-τ plots of both the close bursts of figure 5.2 and distant bursts of figure 5.3, we also see another separation into two distinct populations. These are "escaping" and "remaining" binaries. By escaping, we mean binaries which receive a strong enough kick that they escape the galactic potential – in contrast, remaining binaries remain bound to the galaxy.

Let us consider how the remaining and escaping binaries build up the bimodal population for the close bursts. We have a binary which is escaping the galaxy. This binary can only be observed as a close burst if it has a short lifetime. We see this in figure 5.3: binaries with $v_{\rm com} \gtrsim 200$ km/s all have short lifetimes. Meanwhile, all remaining binaries have the possibility of being observed as close bursts, regardless of lifetime. We produce enough short-lived binaries for them to dominate the population of close bursts, regardless of whether they remain or escape.

What about the distant bursts? Escaping binaries are obviously part of the distant burst population. In the context of the 061201 burst, those with $\tau \cdot v_{\rm com} \approx 34$ kpc are seen as an isodistance line in figure 5.3 (c.f. figure 3.6). There is scatter around the isodistance line due in part to $\sigma_{\rm off}$, in part to the details of initial position and direction of $v_{\rm com}$. If a burst comes from a remaining binary at these distances, the binary must be on a very eccentric orbit and then merge closer to apoapsis. These eccentric binaries can do a number orbits before merging, meaning a large range of lifetimes are possible. If the binary is on an eccentric orbit, they should have received a $v_{\rm com}$ comparable to the galactic rotational velocity. Indeed, seen in figure 5.3 are binaries with a large spread in lifetimes at velocities slightly larger to the rotational velocity $v_{\rm h} = 121.45$ km/s. In fact, most of the distant bursts received velocities at ~ 150 km/s, and some received velocities as small as 100 km/s.

This last point, that a) $v_{\rm com}$ as small as ~ 150 km/s can generate even the most distant bursts and b) it is binaries with $v_{\rm com} \approx 150$ km/s which are most efficient at producing distant bursts, is a key result. It means that it is not necessary to have strong natal kicks to produce the SGRB we have been able to observe. E.g. Tauris et al. (2017) have proposed much smaller kicks, with a $\sigma_{\rm 1D}$ of 50 km/s – meaning kicks of 100 km/s are regularly obtained. These small kicks are specifically proposed for $m_{\rm 1,i} \approx 1.4 M_\odot$. Thus, it is ambiguous to what extent these weak kicks could produce double neutron star binaries

with $v_{\rm com}$ of at least 100 km/s, in the context of our model (see figure 3.1). However, remember that we have neglected the first supernova in the binary in our model, which can potentially boost the system velocity.

Note that there is a strong bias behind our thought of smaller $v_{\rm k}$ producing the largest observed offsets, as there is a strong bias against observing larger offsets. The host galaxies, and hence offsets, of the observed bursts were attributed according to least chance probability. If a binary travels far enough away from its host, we would perceive it to be close enough to another galaxy on the night sky for us to misattribute the host – hence bias against large offset observations (see e.g. Tunnicliffe et al. 2014). As we continue to observe more SGRBs and better understand their distribution, the risk of misattributing a burst grows smaller.

Future extensions

It would be interesting to test the offset distributions from weak kicks. Investigating the $v_{\rm com}$ distribution would tell us how regularly systems with $v_{\rm com} \gtrsim 100$ km/s, that potentially merge at large offsets, are produced. A natural extension is of course to include the first supernova in the system, and see if the chance alignment of the two kicks helps or hinders large system velocities. If that is done, the set of observed SGRBs should also be expanded to include more of the SGRBs observed from spiral galaxies since 2008 to improve statistics.

We could also expand the sample by attempting to model SGRB from elliptical host galaxies. To do so would require a hydrodynamical simulation of the formation of such a galaxy, as the dynamics of a galactic merger will obviously affect the trajectory of a binary within the galaxy. While challenging, such a simulation would also provide two powerful tools: A detailed dynamical and star formation history of the galaxy. The star formation history would give a better constraint on the initial mass of the binary. Together with the dynamic history of the galaxy we would receive a more realistic distribution of offsets of SGRB which are conceivably observable today.

Chapter 7

Conclusion

We have built a model for the dynamical effects of the second supernova in a compact double neutron star binary. After, we synthesize a population of binaries and integrate their trajectories up until they merge, in an environment of spiral galaxies. The produced burst offsets are then compared to observed SGRB offsets. We find that compact binaries separated by more than ~ 20 $R_\odot$ before the second supernova do not merge before Hubble time. No such restrictions were found for the other two free parameters, exploding star mass and natal kick strength. We do however find that natal kicks much weaker than the ones derived from isolated pulsars could potentially be sufficient to produce the sample of burst offsets which we compare to.

Bibliography

Abbott, B. P. et al. (2017), 'Multi-messenger Observations of a Binary Neutron Star Merger', *ApJ* **848**(2), L12.

Bennett, C. L., Larson, D., Weiland, J. L. & Hinshaw, G. (2014), 'The 1% Concordance Hubble Constant', *ApJ* **794**(2), 135.

Church, R. P., Levan, A. J., Davies, M. B. & Tanvir, N. (2011), 'Implications for the origin of short gamma-ray bursts from their observed positions around their host galaxies', *MNRAS* **413**, 2004–2014.

Davies, M. B. (1995), 'The binary zoo: the calculation of production rates of binaries through 2+1 encounters in globular clusters', *MNRAS* **276**(3), 887–905.

Davies, M. B., Ritter, H. & King, A. (2002), 'Formation of the binary pulsars J1141-6545 and B2303+46', *MNRAS* **335**(2), 369–376.

Eggleton, P. P. (1983), 'Aproximations to the radii of Roche lobes.', *ApJ* **268**, 368–369.

Fong, W., Berger, E. & Fox, D. B. (2010), 'Hubble Space Telescope Observations of Short Gamma-Ray Burst Host Galaxies: Morphologies, Offsets, and Local Environments', *ApJ* **708**(1), 9–25.

Hobbs, G., Lorimer, D. R., Lyne, A. G. & Kramer, M. (2005), 'A statistical study of 233 pulsar proper motions', *MNRAS* **360**, 974–992.

Hurley, J. R., Pols, O. R. & Tout, C. A. (2000), 'Comprehensive analytic formulae for stellar evolution as a function of mass and metallicity', *MNRAS* **315**, 543–569.

Kouveliotou, C., Meegan, C. A., Fishman, G. J., Bhat, N. P., Briggs, M. S., Koshut, T. M., Paciesas, W. S. & Pendleton, G. N. (1993), 'Identification of Two Classes of Gamma-Ray Bursts', *ApJ* **413**, L101.

Lai, D., Chernoff, D. F. & Cordes, J. M. (2001), 'Pulsar Jets: Implications for Neutron Star Kicks and Initial Spins', *ApJ* **549**(2), 1111–1118.

Lorimer, D. R. (2008), 'Binary and Millisecond Pulsars', *Living Reviews in Relativity* **11**, 8.

Ruderman, M. (1975), Theories of gamma -ray bursts., *in* P. G. Bergman, E. J. Fenyves & L. Motz, eds, 'Seventh Texas Symposium on Relativistic Astrophysics', Vol. 262, pp. 164–180.

Salpeter, E. E. (1955), 'The Luminosity Function and Stellar Evolution.', *ApJ* **121**, 161.

Tauris, T. M., Kramer, M., Freire, P. C. C., Wex, N., Janka, H. T., Langer, N., Podsiadlowski, P., Bozzo, E., Chaty, S., Kruckow, M. U., van den Heuvel, E. P. J., Antoniadis, J., Breton, R. P. & Champion, D. J. (2017), 'Formation of Double Neutron Star Systems', *ApJ* **846**(2), 170.

Taylor, J. H. & Weisberg, J. M. (1982), 'A new test of general relativity - Gravitational radiation and the binary pulsar PSR 1913+16', *ApJ* **253**, 908–920.

Thomas, J., Saglia, R. P., Bender, R., Thomas, D., Gebhardt, K., Magorrian, J., Corsini, E. M. & Wegner, G. (2009), 'Dark Matter Scaling Relations and the Assembly Epoch of Coma Early-Type Galaxies', *ApJ* **691**, 770–782.

Tunnicliffe, R. L., Levan, A. J., Tanvir, N. R., Rowlinson, A., Perley, D. A., Bloom, J. S., Cenko, S. B., O'Brien, P. T., Cobb, B. E., Wiersema, K., Malesani, D., de Ugarte Postigo, A., Hjorth, J., Fynbo, J. P. U. & Jakobsson, P. (2014), 'On the nature of the 'hostless' short GRBs', *MNRAS* **437**(2), 1495–1510.

Wright, E. L. (2006), 'A Cosmology Calculator for the World Wide Web', *PASP* **118**(850), 1711–1715.

Appendix A

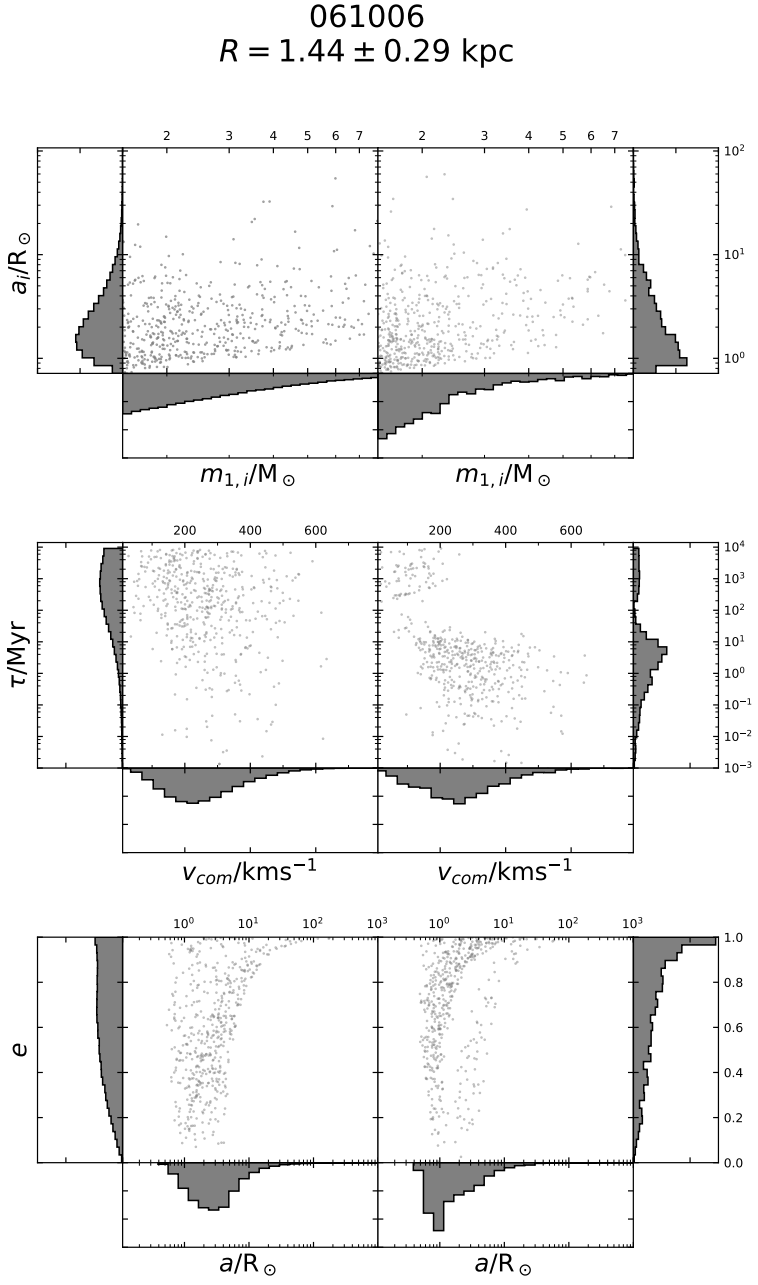
061006
$R = 1.44 \pm 0.29$ kpc
$a_i/\mathrm{R}_\odot$
$m_{1,i}/\mathrm{M}_\odot$
$m_{1,i}/\mathrm{M}_\odot$
τ/Myr
$v_{com}/\mathrm{kms}^{-1}$
$v_{com}/\mathrm{kms}^{-1}$
e
$a/\mathrm{R}_\odot$
$a/\mathrm{R}_\odot$

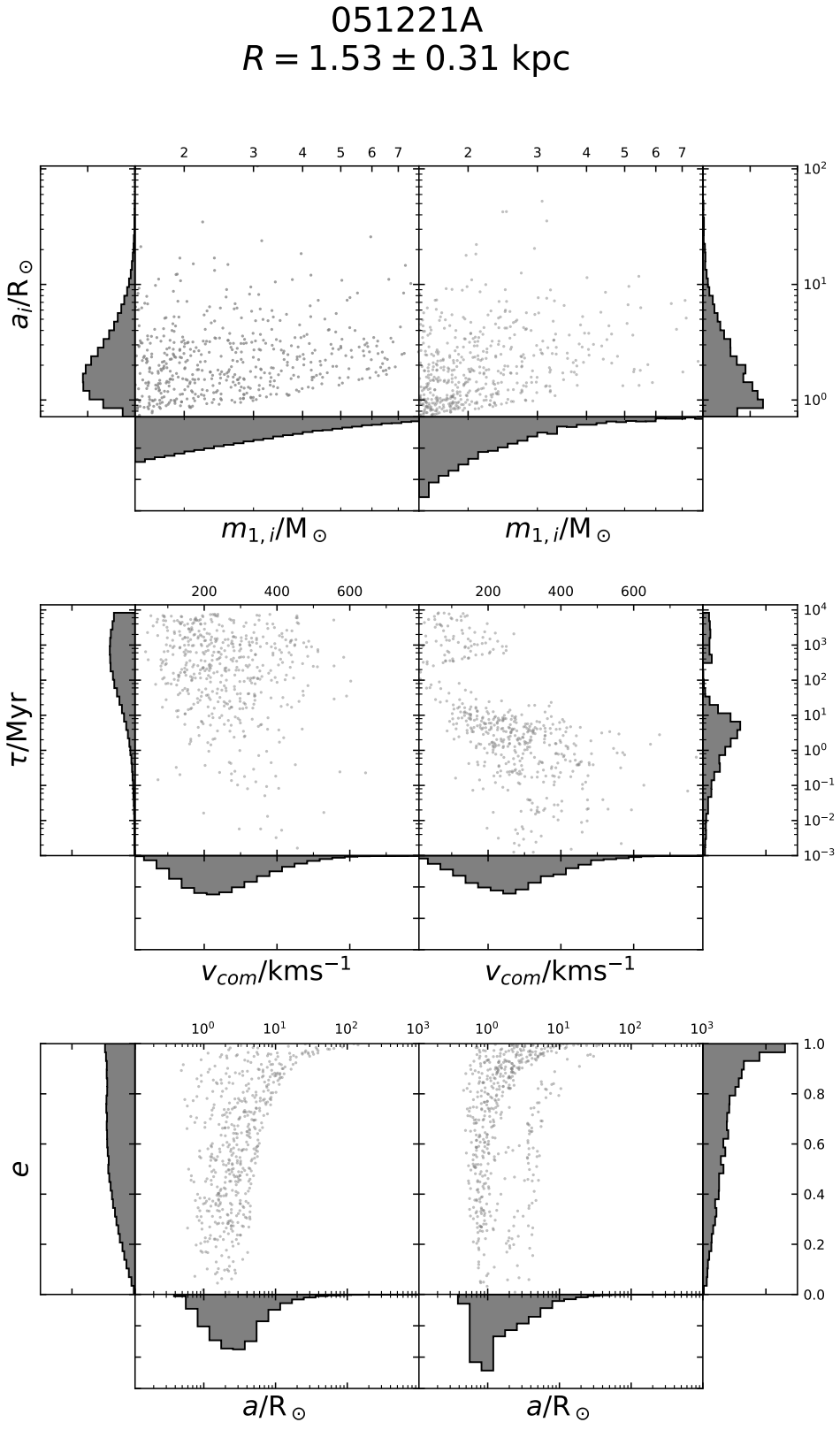
051221A
$R = 1.53 \pm 0.31$ kpc
$a_i/\mathrm{R}_\odot$
$m_{1,i}/\mathrm{M}_\odot$
$m_{1,i}/\mathrm{M}_\odot$
τ/Myr
$v_{com}/\mathrm{kms}^{-1}$
$v_{com}/\mathrm{kms}^{-1}$
e
$a/\mathrm{R}_\odot$
$a/\mathrm{R}_\odot$

070714B
$R = 3.08 \pm 0.47$ kpc

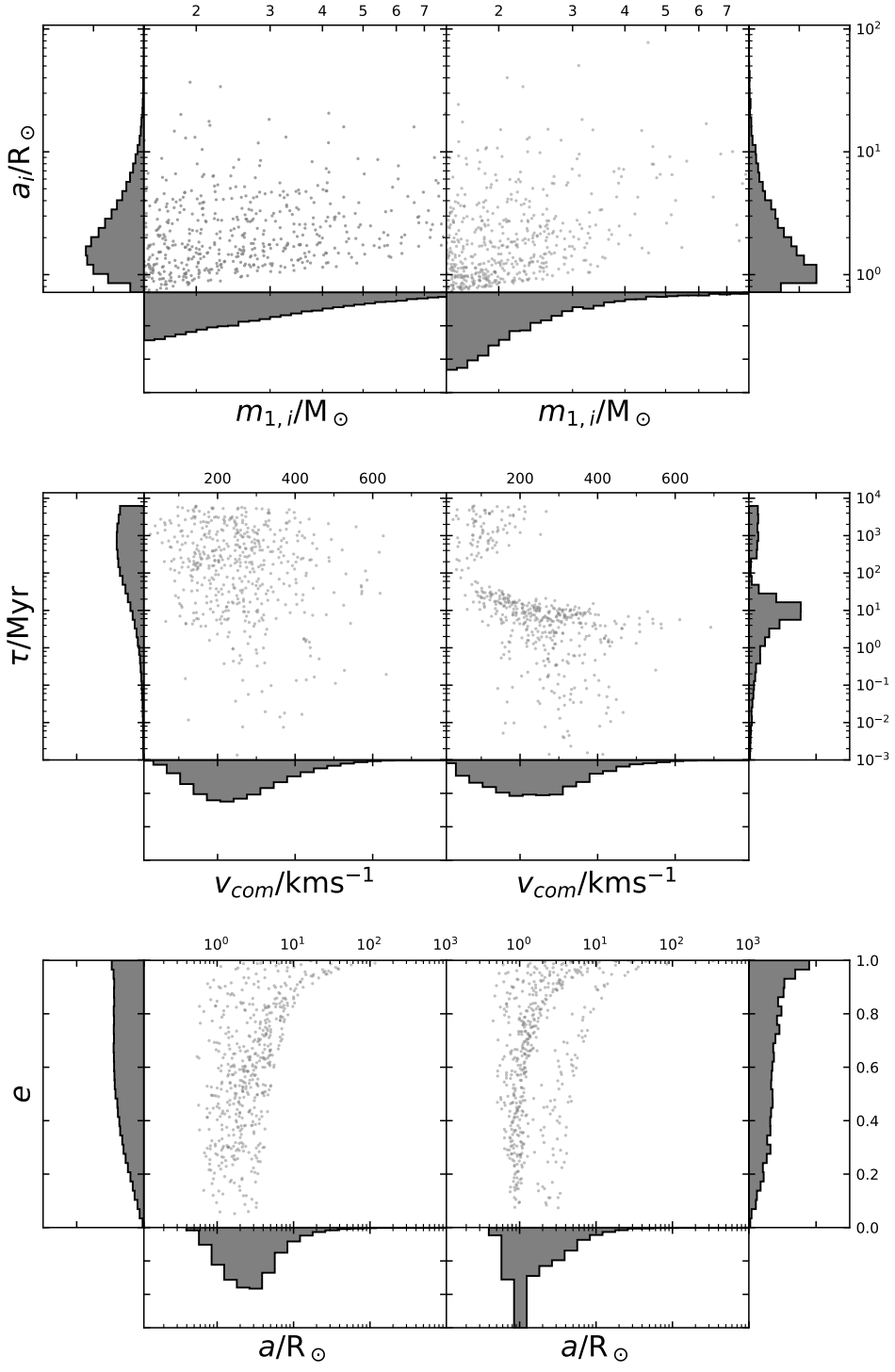

070429B
$R = 4.7 \pm 4.7$ kpc

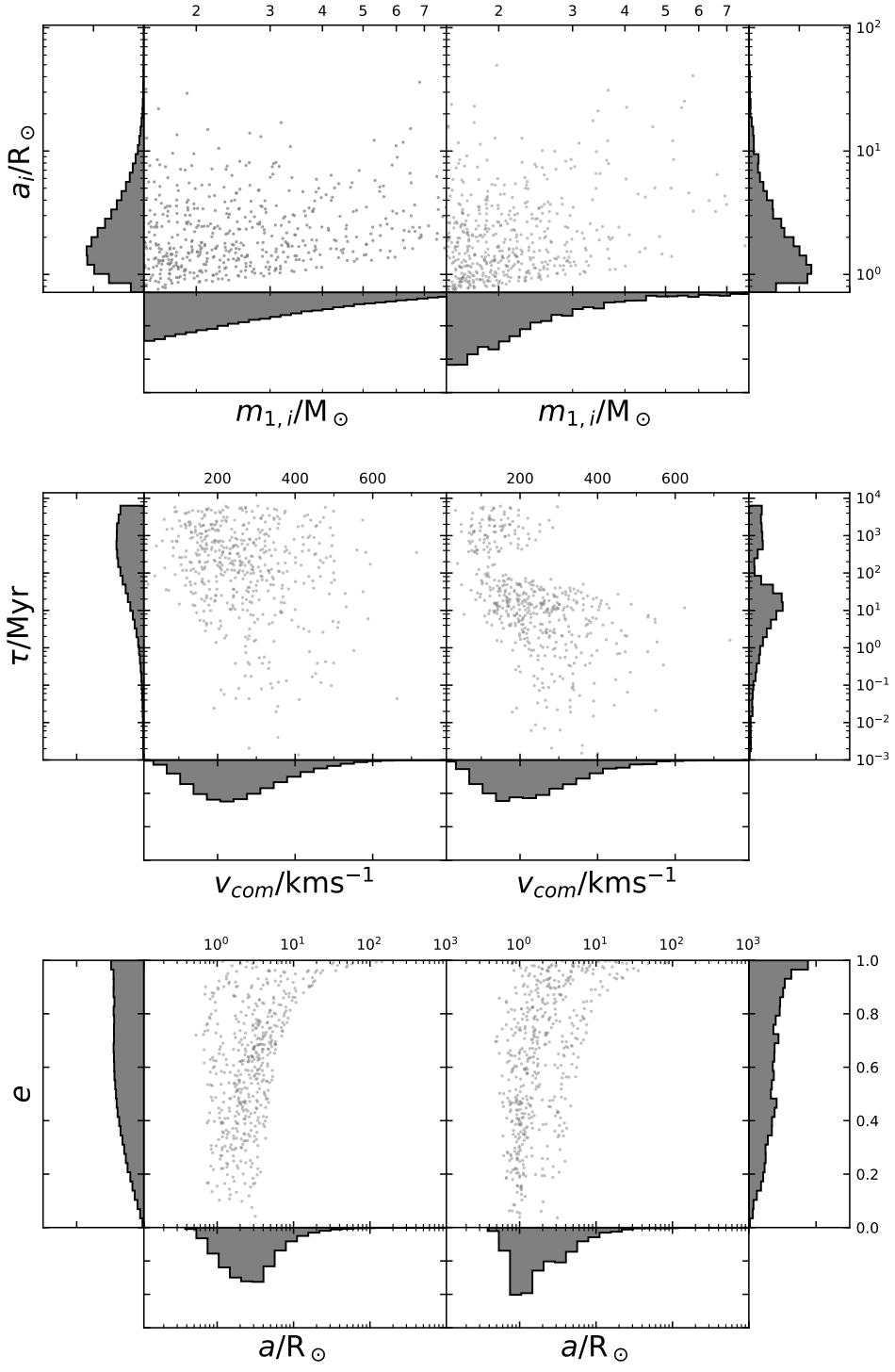

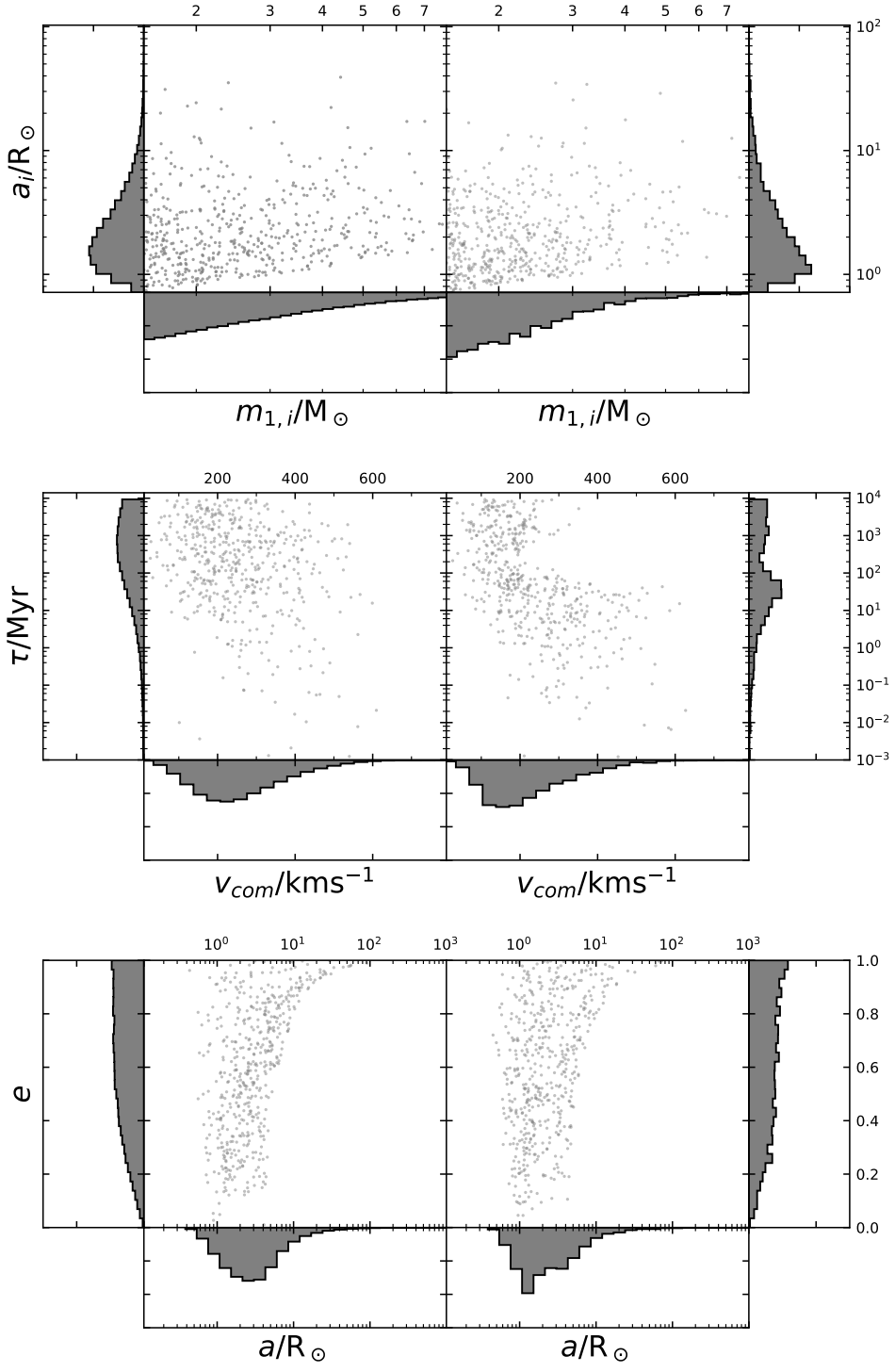
061210
$R = 10.7 \pm 6.9$ kpc
$a_i/\mathrm{R}_\odot$
$m_{1,i}/\mathrm{M}_\odot$
$m_{1,i}/\mathrm{M}_\odot$
τ/Myr
$v_{com}/\mathrm{kms}^{-1}$
$v_{com}/\mathrm{kms}^{-1}$
e
$a/\mathrm{R}_\odot$
$a/\mathrm{R}_\odot$

071227
$R = 16.1 \pm 0.2$ kpc

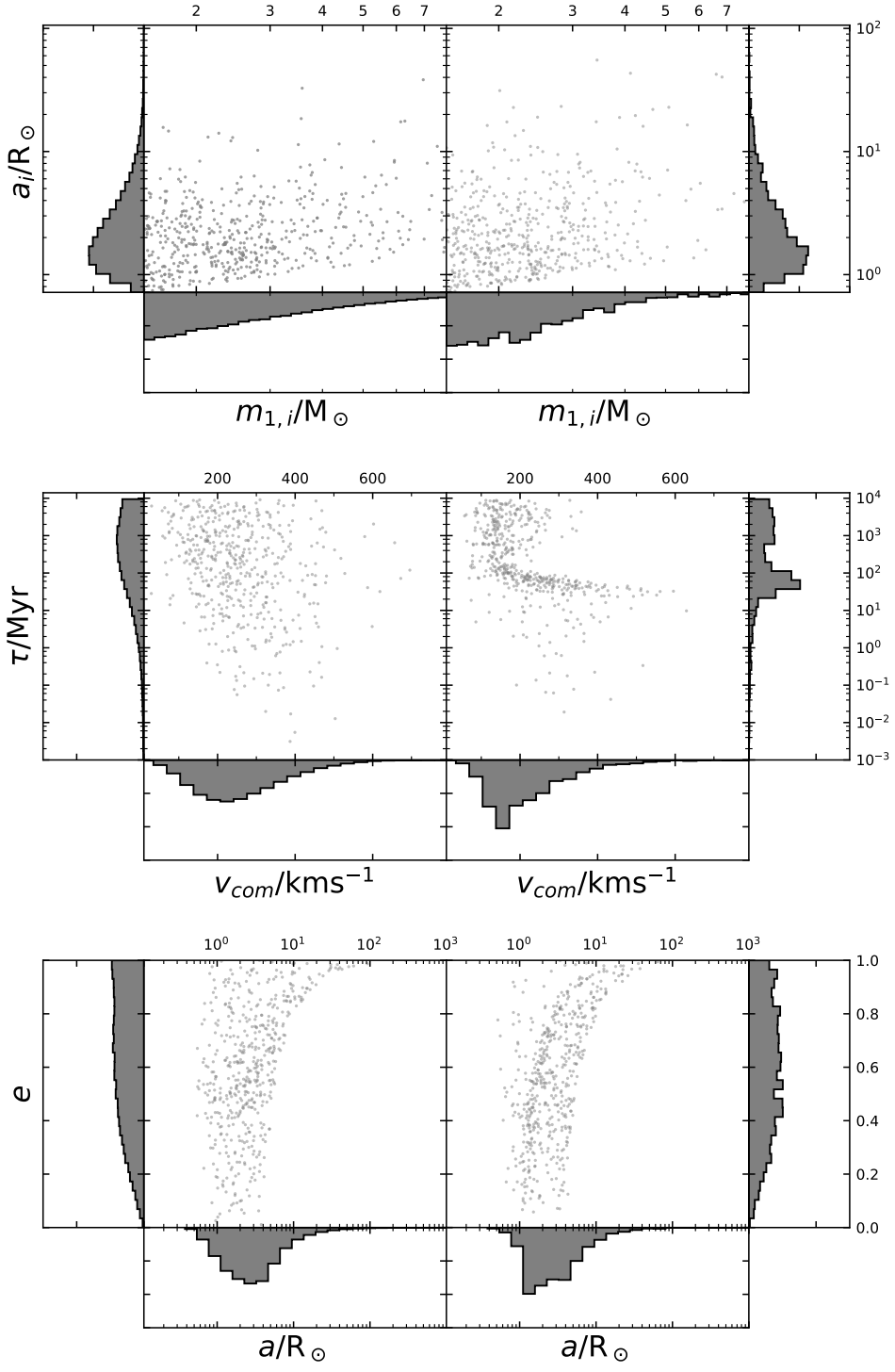

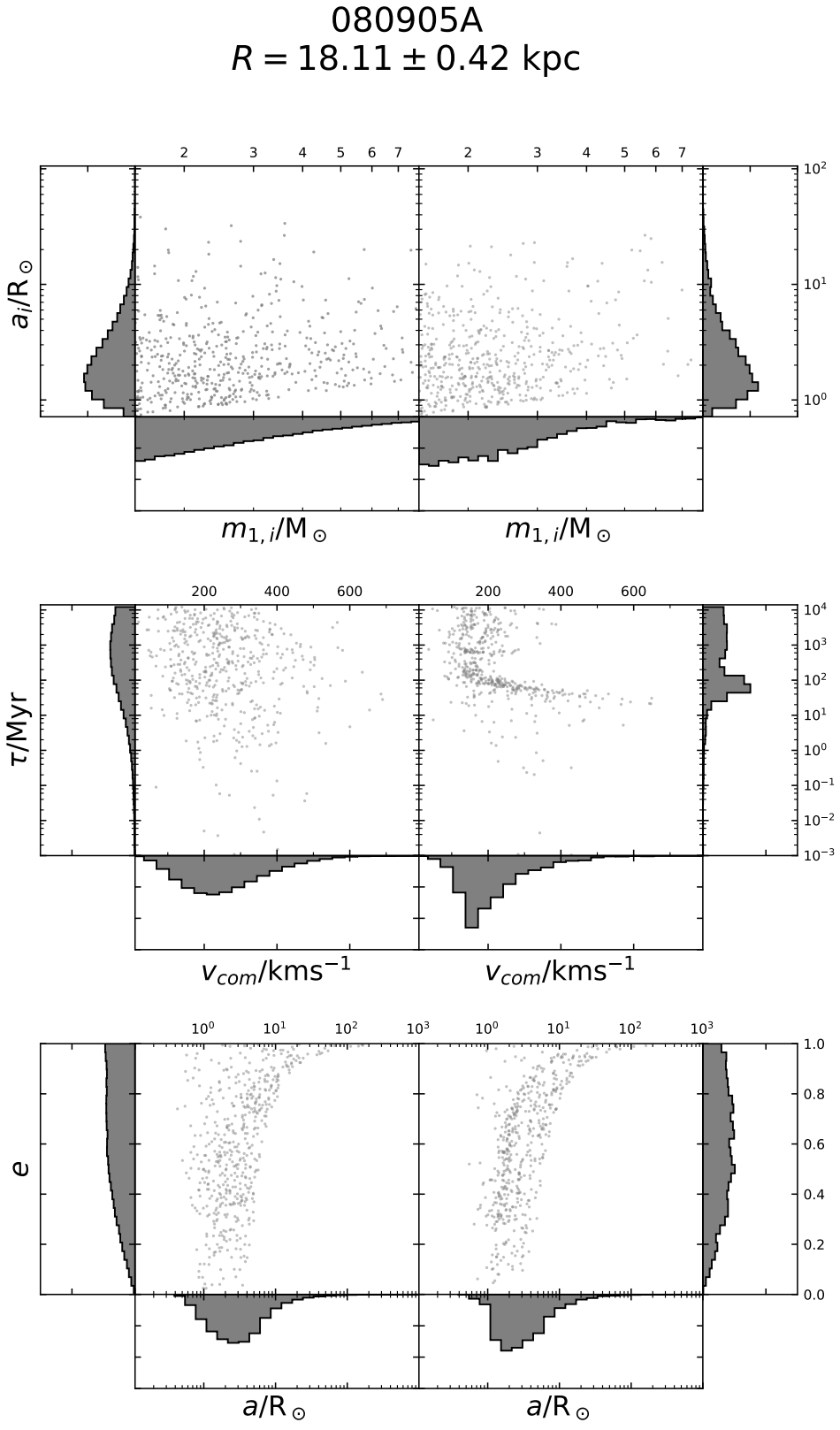
080905A
$R = 18.11 \pm 0.42$ kpc
$a_i/\mathrm{R}_\odot$
$m_{1,i}/\mathrm{M}_\odot$
$m_{1,i}/\mathrm{M}_\odot$
τ/Myr
$v_{com}/\mathrm{kms}^{-1}$
$v_{com}/\mathrm{kms}^{-1}$
e
$a/\mathrm{R}_\odot$
$a/\mathrm{R}_\odot$

070809
$R = 19.61 \pm 1.9$ kpc

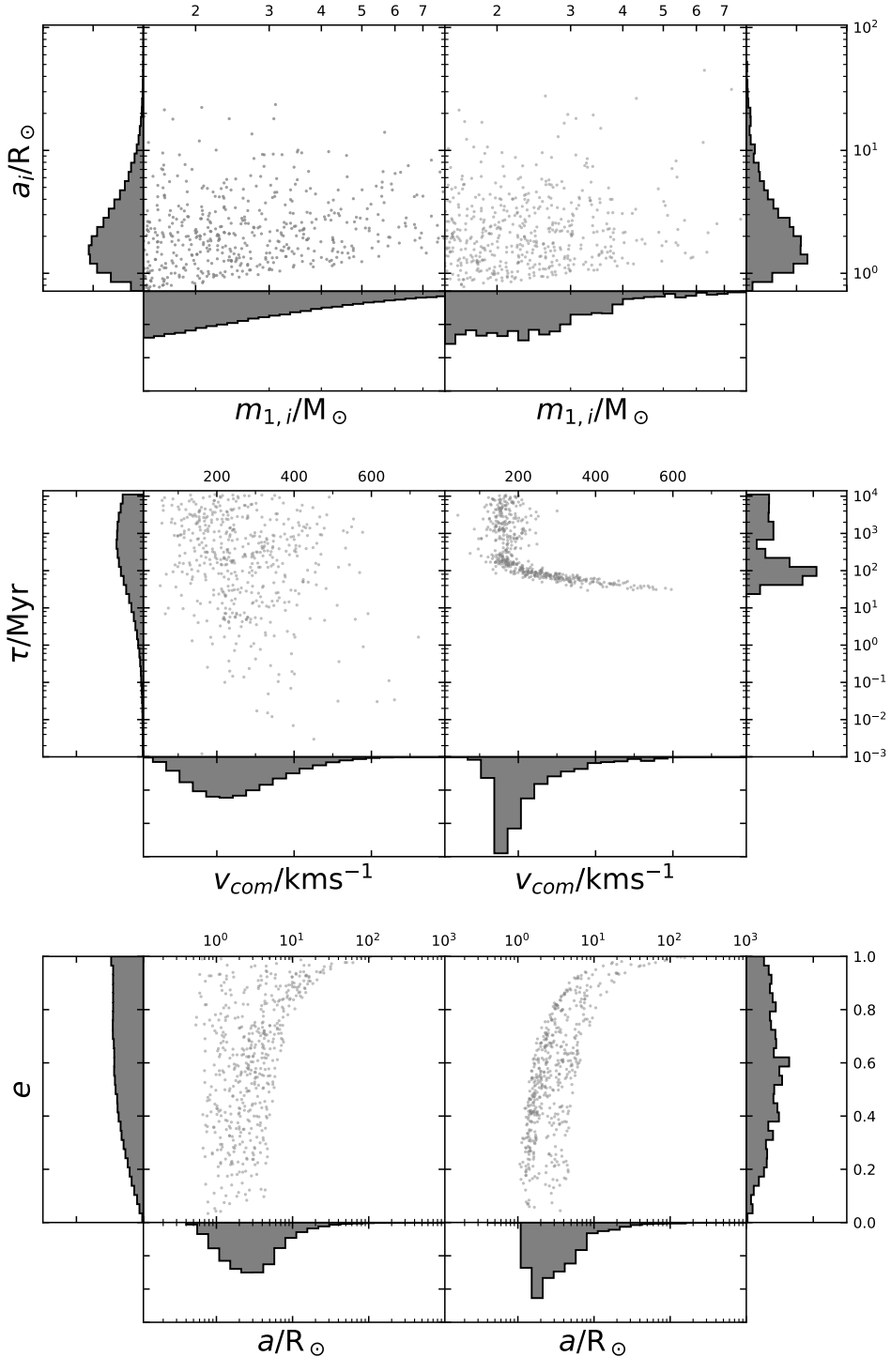

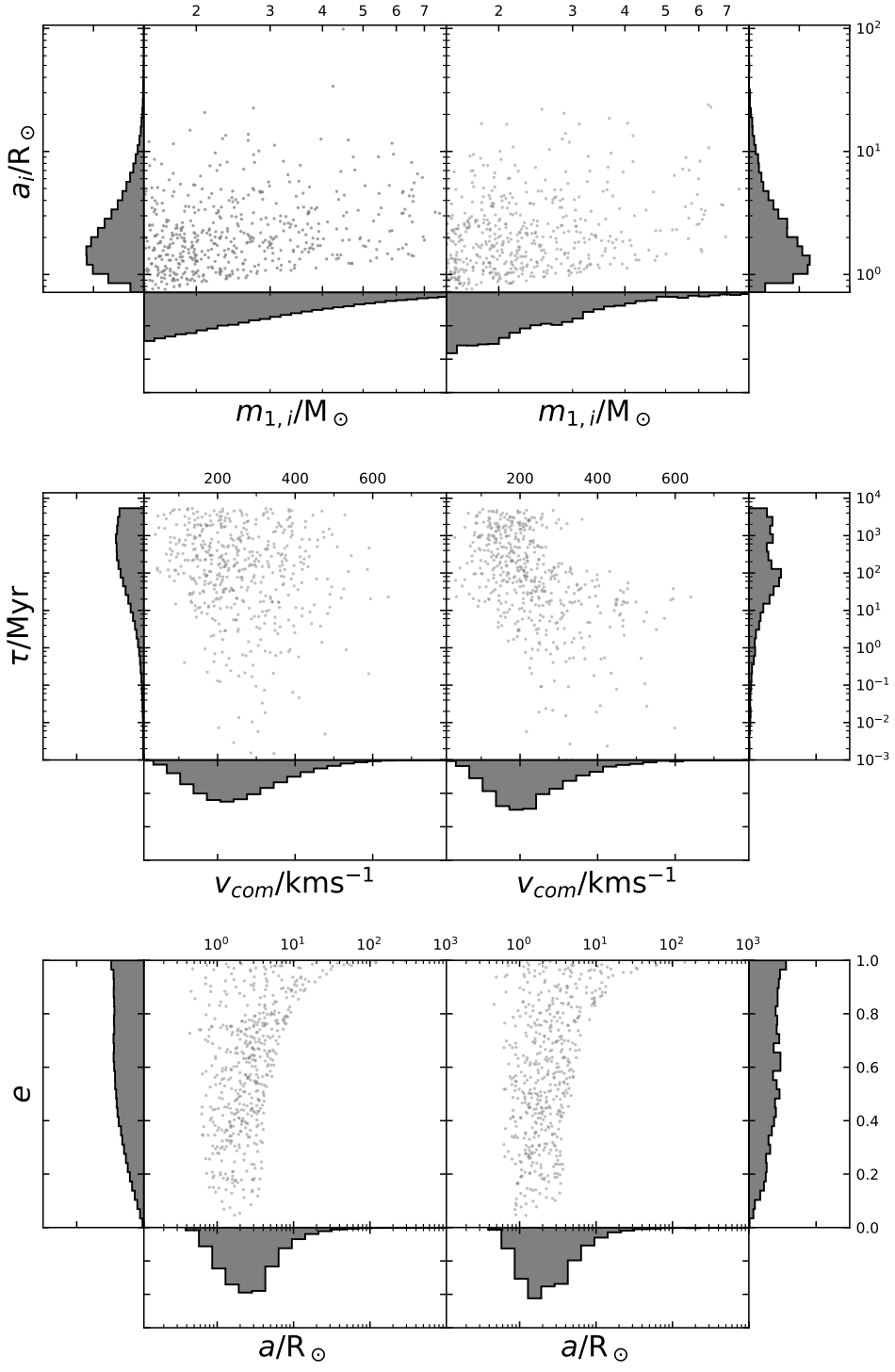
060801
$R = 19.7 \pm 14$ kpc
$a_i/\mathrm{R}_\odot$
$m_{1,i}/\mathrm{M}_\odot$
$m_{1,i}/\mathrm{M}_\odot$
τ/Myr
$v_{com}/\mathrm{kms}^{-1}$
$v_{com}/\mathrm{kms}^{-1}$
e
$a/\mathrm{R}_\odot$
$a/\mathrm{R}_\odot$

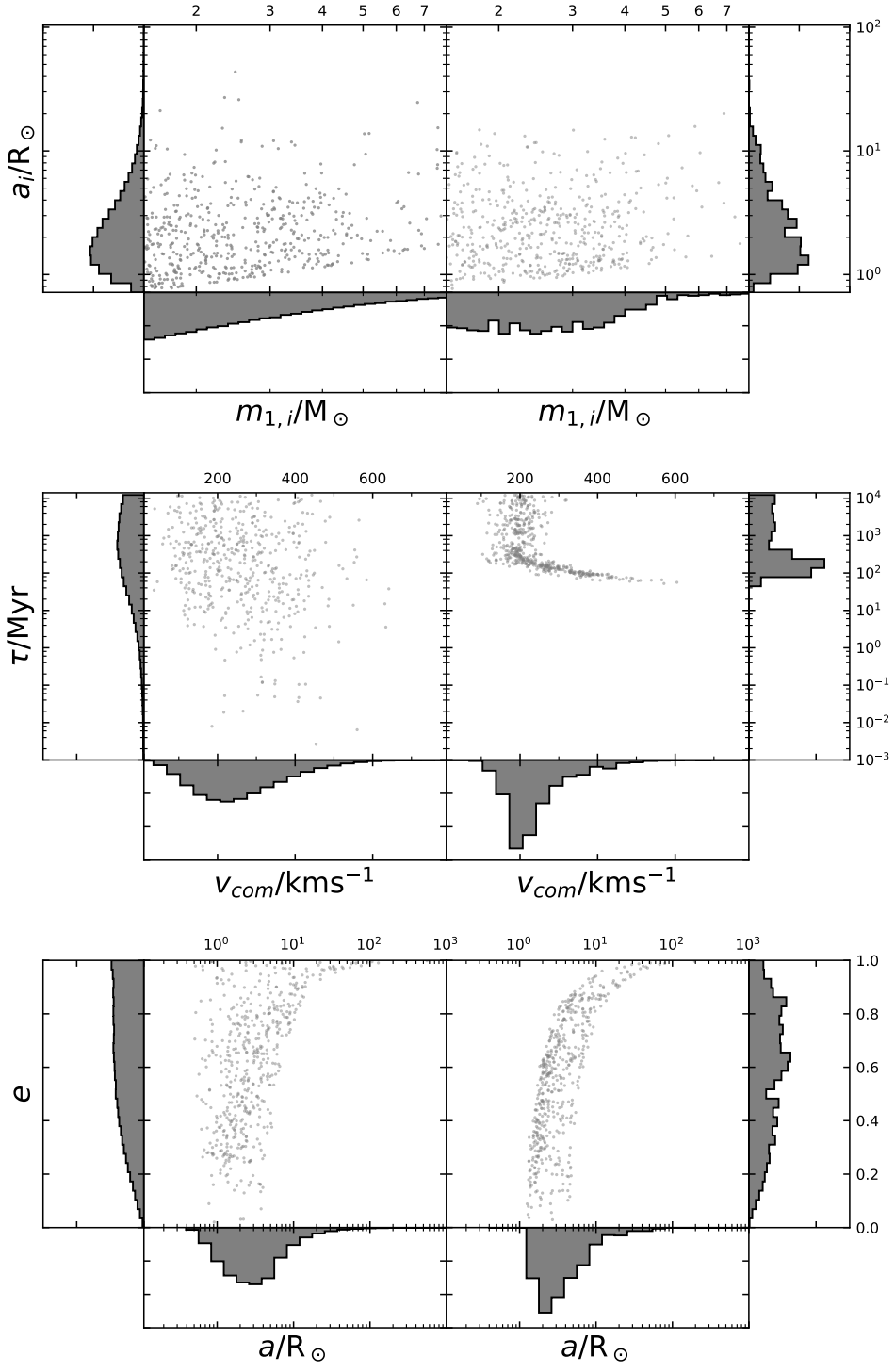
061201
$R = 33.9 \pm 0.4$ kpc
$a_i/\mathrm{R}_\odot$
$m_{1,i}/\mathrm{M}_\odot$
$m_{1,i}/\mathrm{M}_\odot$
τ/Myr
$v_{com}/\mathrm{kms}^{-1}$
$v_{com}/\mathrm{kms}^{-1}$
e
$a/\mathrm{R}_\odot$
$a/\mathrm{R}_\odot$

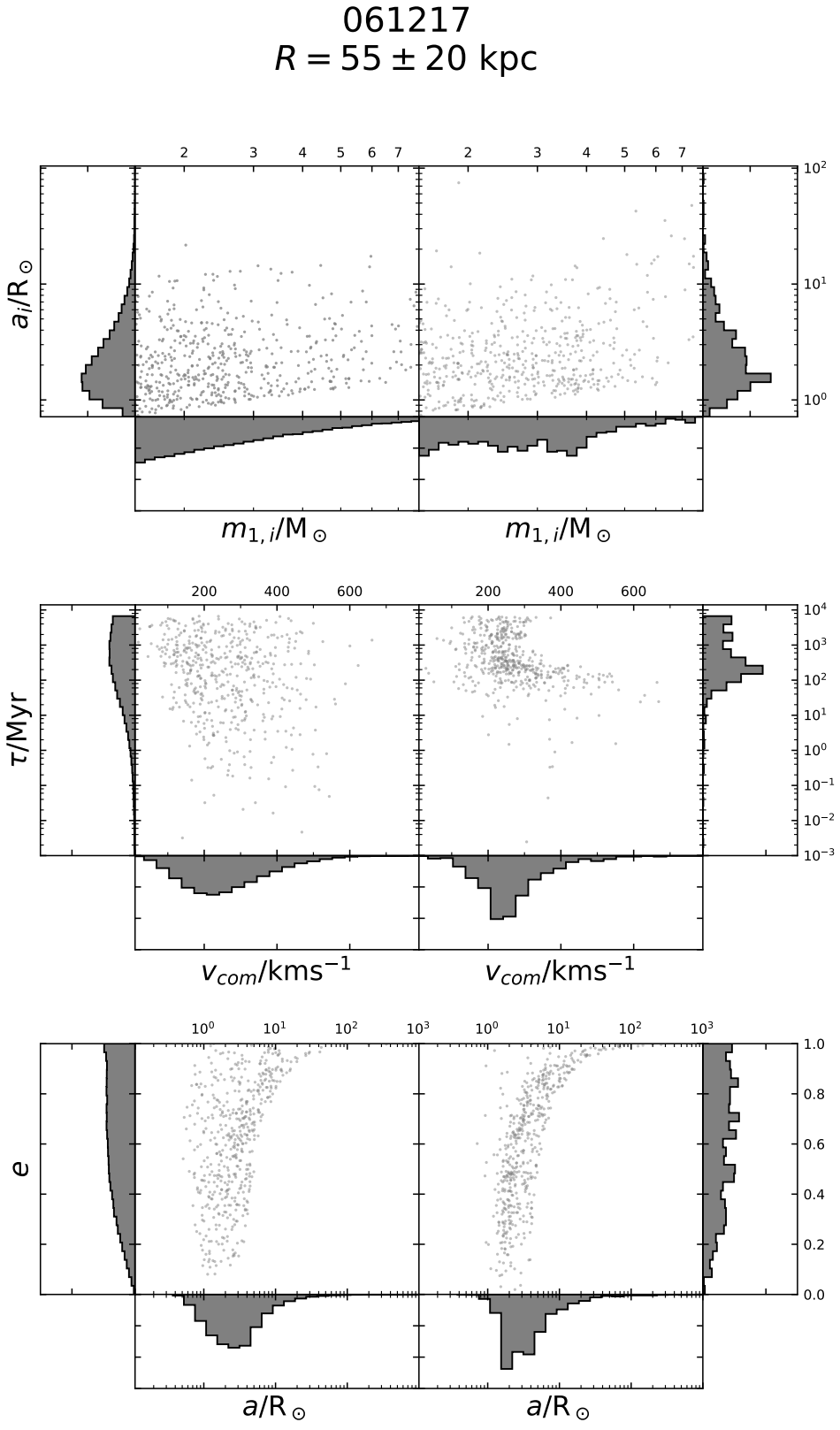
061217
$R = 55 \pm 20$ kpc
$a_i/\mathrm{R}_\odot$
$m_{1,i}/\mathrm{M}_\odot$
$m_{1,i}/\mathrm{M}_\odot$
τ/Myr
$v_{com}/\mathrm{kms}^{-1}$
$v_{com}/\mathrm{kms}^{-1}$
e
$a/\mathrm{R}_\odot$
$a/\mathrm{R}_\odot$